A Feature Complementary Attention Network Based on Adaptive Knowledge Filtering for Hyperspectral Image Classification

Cuiping Shi[ID], *Member, IEEE*, Haiyang Wu[ID], and Liguo Wang[ID], *Member, IEEE*

Abstract— In recent years, convolutional neural networks (CNNs) have been widely used in hyperspectral image classification (HSIC). However, the size of the convolutional kernel in CNNs is fixed, which makes it difficult to capture the dependence of long-range feature information. In addition, the extracted features often contain a large amount of redundant information. In order to alleviate these issues, a feature complementary attention network based on adaptive knowledge filtering (FCAN_AKF) is proposed in this article. First, in order to alleviate the problem that CNNs are difficult to capture the dependence between close-range and long-range spectral features due to the limited receptive field, a nonlocal band regrouping (NBR) strategy is designed. NBR enables CNN to capture nonlocal spectral features in a limited receptive field to establish the interdependence between close-range and long-range spectral features. In addition, the nonlocal features extracted after using NBR and the local features of the original hyperspectral image are integrated to achieve complementation between nonlocal features and local features. Then, in order to eliminate the interference of redundant information on the network, a dual-pyramid spectral–spatial attention (DPSSA) module is proposed and used to capture spectral–spatial attention. Next, an adaptive knowledge filter (AKF) is designed, which can adaptively further filter out redundant information and enhance feature information that is beneficial for classification. Finally, extensive experiments were conducted on three challenging datasets, demonstrating that the proposed method has stronger competitiveness compared to some state-of-the-art HSIC methods.

Index Terms— Adaptive knowledge filter (AKF), convolutional neural network (CNN), dual-pyramid spectral–spatial attention (DPSSA), hyperspectral image classification (HSIC), nonlocal band regrouping (NBR).

Cuiping Shi is with the College of Information Engineering, Huzhou University, Huzhou 313000, China, and also with the Department of Communication Engineering, Qiqihar University, Qiqihar 161000, China (e-mail: shicuiping@qqhru.edu.cn).

Haiyang Wu is with the Department of Communication Engineering, Qiqihar University, Qiqihar 161000, China (e-mail: 2021910323@qqhru.edu.cn).

Liguo Wang is with the College of Information and Communication Engineering, Dalian Nationalities University, Dalian 116000, China (e-mail: wangliguo@hrbeu.edu.cn).

I. Introduction

WITH the rapid development of hyperspectral remote sensing technology, hyperspectral images (HSIs) have been applied to more and more fields [1], [2], for example, coastal environmental monitoring [3], ecosystem protection [4], crop monitoring [5], [6], [7], [8], and medical diagnosis [9], [10]. The premise of these applications is that the ground objects in HSIs are accurately identified and classified. In the early days, some classic machine learning methods were mainly used for hyperspectral image classification (HSIC), for example, distance classifier [11], maximum likelihood classifier [12], and sparse representation classification (SRC) [13], [14]. Although these methods have simple principles and are easy to implement, they overly rely on manual features and prior information, resulting in poor generalization. In addition, among these methods, only spectral information is used for classification, and the importance of spatial information in HSIs is ignored, which limits their classification performance.

In the past decade, convolutional neural networks (CNNs) have gradually become a research hotspot in HSIC [15], [16], [17]. The features of HSIs can be autonomously fit through the training of CNNs, while the traditional manual feature method is avoided, thereby improving the generalization of the network. In [18], a deep convolutional network was used for HSIC. Since hundreds of spectral bands are included in each pixel of the HSIs, there are significant differences in the spectral features of pixels corresponding to different ground objects. Therefore, each pixel of the HSIs is considered as a 1-D speech signal input by this method, and a 1-D convolutional neural network (1D-CNN) is used to extract spectral features of the HSIs. Finally, a more competitive classification performance compared to classical classifiers was achieved by this method. However, HSIs are prone to external interference during imaging, and spectral information between different ground objects is not completely separated. Therefore, not only the spectral features need to be extracted for HSIC, but also the extraction of spatial features needs to be paid attention to. In [19], a 3-D convolutional neural network (3D-CNN) was proposed. The 3-D convolution is used by this method to simultaneously extract spatial–spectral features of HSIs, which significantly improves the classification performance compared to 1D-CNN. In early CNNs, convolutional layers were directly stacked to improve the classification performance of HSIs, which easily led to over-fitting of the network.

To this end, a spectral–spatial residual network (SSRN) was proposed [20]. SSRN constructs a network through residual structure, and the deep features of HSIs can be better extracted. In addition, in [21], a fast dense connection network was proposed, and the same feature of HSIs was multiplexed through dense connection to avoid over-fitting of the network.

Recently, in order to extract important features of HSIs, a series of attention mechanism [22], [23], [24], [25] networks has been applied to HSIC. In [26], two different branches were used to capture the spatial and spectral attention of HSIs, avoiding mutual interference of spatial–spectral information. In [27], a double-branch dual attention (DBDA) network was proposed. Similar to [26], in DBDA, spatial–spectral attention is also captured through two different branches. The difference is that the spatial–spectral features of DBDA are captured through adaptive self-attention, and better classification performance is achieved. Subsequently, a self-attention network using a network search strategy was proposed [28]. The optimal structure of the network for this method is determined by the network framework search strategy to achieve the optimal classification results. In order to fully utilize the multiscale features of HSIs, a hierarchical residual attention network was proposed [29]. However, due to the sensitivity of convolutional kernels to spatial rotation, the classification performance of conventional attention networks in rotated HSIs is poor. For this reason, a rotation invariant attention network (RIAN) was proposed [30], and the rotation invariant spatial–spectral attention was extracted by RIAN using a correction attention module, which effectively alleviated the problem of spatial rotation. In addition, in order to capture the bidirectional correlation of the internal spectral of HSIs, an attention network based on bidirectional short-term memory was proposed [31].

Although some problems have been solved by these methods, there are still some challenges in the application of CNNs in HSIC.

1) The receptive field of CNNs is limited by the size of the convolution kernel, and it is difficult for the limited receptive field to capture the interdependence between the close-range spectral information and the long-range spectral information.

2) Although the attention mechanism can suppress some redundant information, there is still some redundant information in the features extracted by CNNs. This redundant information can affect the judgment of the network, limiting its classification performance.

For the first challenge, some transformer-based classification methods were used in HSIC in the past two years [32], [33], [34], [35], [36]. Considering the transformer's strong sensitivity to capturing contextual correlations, it has been introduced into HSIC to capture the interdependence between close-range and long-range spectral information. In [37], a SpectralFormer network was proposed. In this method, the spectral band was first regarded as a long sequence, and then, the transformer network was used to capture the correlation of spectral context. Although spectral contextual information can be effectively learned by SpectralFormer, the local information of HSIs is ignored. Therefore, some HSIC

methods that integrate CNN and transformer were proposed to combine local and nonlocal features of HSIs. In [38], HSIs were effectively classified by combining CNN with transformer. Although the interdependence between close-range spectral information and long-range spectral information can be established by these methods, the interference of redundant information on the network has not been effectively addressed.

In order to alleviate these issues, a feature complementary attention network based on adaptive knowledge filtering (FCAN_AKF) is proposed in this article. First, aiming at the problem of limited receptive field of CNNs, a nonlocal band regrouping (NBR) strategy was designed. NBR achieves the interaction between close-range spectral information and long-range spectral information by regrouping spectral information. In addition, two different branches are used to extract nonlocal features after NBR and local features of the original HSIs to achieve complementary features. Then, in order to suppress the interference of redundant information on the network, a dual-pyramid spectral–spatial attention (DPSSA) module is proposed to capture spectral–spatial attention. Next, an adaptive knowledge filter (AKF) is designed to further remove redundant information and enhance important feature information.

The main contributions of this article include the following three parts.

1) In order to establish the interdependence between close-range spectral information and long-range spectral information of HSIs under a limited receptive field, an NBR strategy is proposed. In addition, two different branches are used to extract nonlocal features and local features, respectively, in order to achieve complementary features in HSIs.

2) A DPSSA module is designed. The spectral–spatial attention is modeled by DPSSA in an autocorrelation manner. And a multiscale pooling pyramid is embedded in attention to reduce information loss during feature extraction.

3) An AKF is designed. Redundant information is adaptively removed by AKF through network training iterations, and feature information that is beneficial for classification is enhanced.

The rest of this article is arranged as follows. In Section II, the overall framework of FCAN_AKF, NBR, DPSSA, and AKF is discussed in detail. In Section III, three HSI datasets and some hyperparameter settings of the network are introduced in detail. Then, NBR, DPSSA, and AKF are conducted some ablation experiments. Finally, the effectiveness of FCAN_AKF is verified. In Section IV, the conclusions are given.

II. METHODOLOGY

In order to capture the interdependence between close-range spectral information and long-range spectral information, and alleviate the interference of redundant information on the network to achieve effective classification of HSIs, an FCAN_AKF is proposed. First, an NBR strategy is proposed, and two different branches are used to extract nonlocal features from NBR and local features from the original
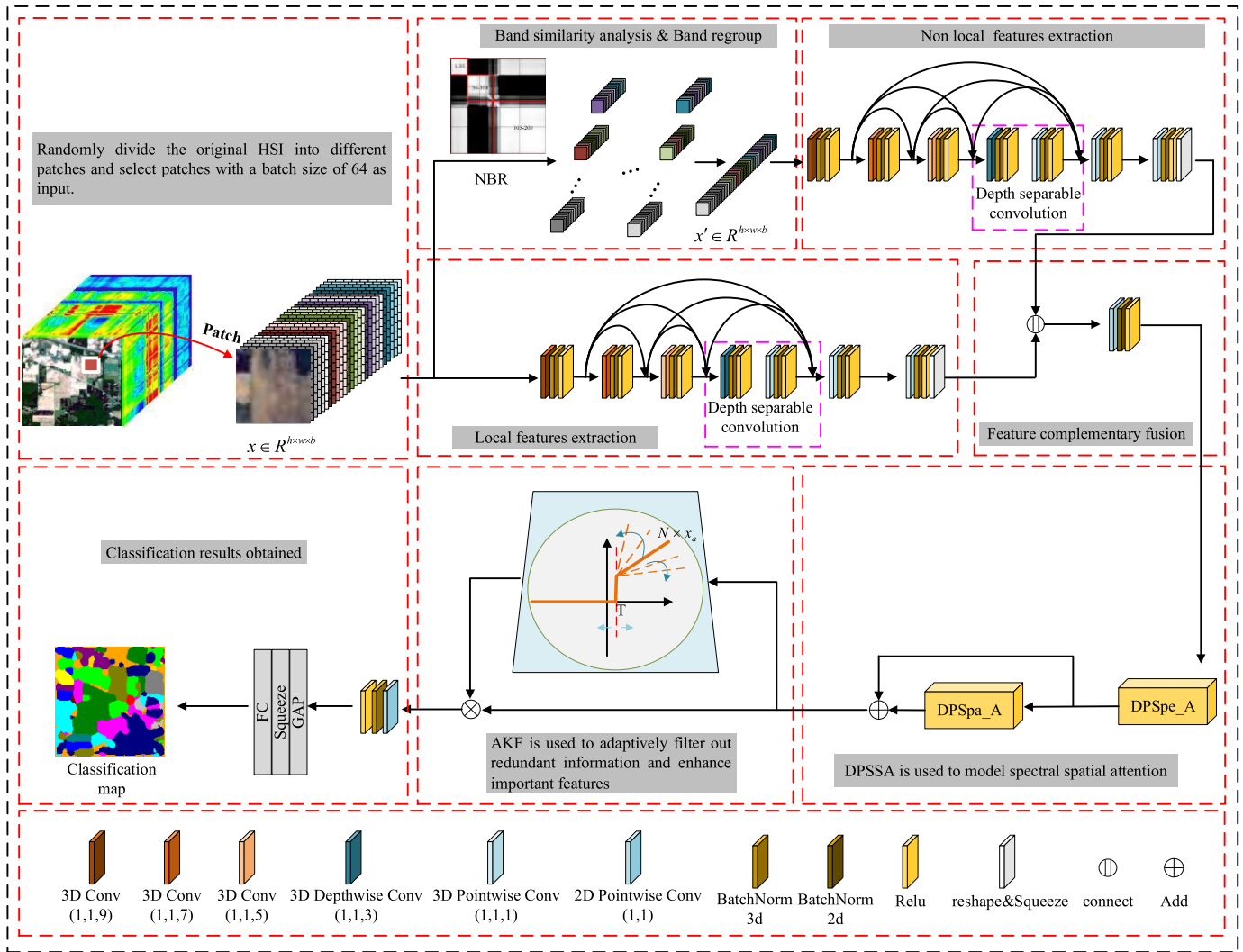
Fig. 1. Overall framework of FCAN_AKF.

image to achieve feature complementary. Then, a DPSSA is used to capture spectral–spatial attention. Finally, an AKF was designed to further alleviate the interference of redundant information. In this section, the overall framework of FCAN_AKF, NBR, DPSSA, and AKF will be introduced in detail.

A. Overall Framework of FCAN_AKF

The proposed FCAN_AKF network is shown in Fig. 1. Specifically, FCAN_AKF takes patches as input. Therefore, the original HSIs are first divided into different patches, and the patches are input in a batch size of 64. Then, in order to make the network establish the long-range interaction relationship of spectral features under the limited receptive field, an NBR strategy is proposed. NBR first analyzes the correlation between spectral bands and groups them based on the correlation. Then, the spectrum in each group are regrouped again to enable the network to capture the interdependence between close-range spectral information and long-range spectral information. In addition, in order to achieve complementary between nonlocal features and local features, two branches

Layer Number	Type	Size	Normalization	Activation
Layer 1	3D Conv	$(1 \times 1 \times 9)$	3D BN	Relu
Layer 2	3D Conv	$(1 \times 1 \times 7)$	3D BN	Relu
Layer 3	3D Conv	$(1 \times 1 \times 5)$	3D BN	Relu
Layer 4	DSC Conv	—	3D BN	Relu
Layer 5	3D Conv	$(1 \times 1 \times 1)$	3D BN	Relu
Layer 6	3D Conv	$(1 \times 1 \times 1)$	3D BN	Relu

Fig. 2. Detailed network structure of nonlocal feature extraction and local feature extraction.

are designed to extract nonlocal features after band regrouping and local features of the original HSIs, respectively. In order to simplify the network, the network structure for extracting nonlocal features and the network structure for extracting local features adopt the same construction. The detailed structure is shown in Fig. 2.

In detail, 3-D convolution kernels of multiple scales are used to extract spectral–spatial features at the same time, and the dense connection structure is combined to multiplex the same feature, avoiding network over-fitting. In addition, deep

separable convolutions (DSCs) are also embedded to reduce network parameters. Specifically, in DSC, a 3-D depthwise convolution is first utilized to extract the features of input channels one by one, and then, a 3-D pointwise convolution is adopted for channel feature fusion. Compared with conventional convolutions, DSC can significantly reduce the number of network parameters while ensuring the same classification performance. Then, a pointwise convolutional layer is used to fuse local and nonlocal features. The continuous operations of 2-D pointwise convolution, BatchNorm, and rectified linear unit (ReLU) are included in the pointwise convolution layer. Next, a DPSSA was used to model spectral–spatial attention. DPSSA includes dual-pyramid spectral attention (DPSpe_A) and dual-pyramid spatial attention (DPSpa_A). In general, DPSpe_A is first used to capture spectral attention by DPSSA, and then, DPSpa_A is used to model spatial attention. In order to better integrate spectral–spatial attention, a residual structure was introduced into DPSSA. Subsequently, in order to further eliminate the interference of redundant information, an AKF was designed. AKF can adaptively filter out redundant information that interferes with network classification and gain information that is beneficial for classification by iteratively updating parameters N and T through network training. Specifically, T and N here represent the threshold and gain values of AKF, respectively. Finally, classification is carried out through the fully connected layer.

B. NBR Strategy

In the research field of HSIC, the extraction of spectral information is extremely crucial. As shown in Fig. 3, the spectral curves corresponding to different ground objects in the HSIs are not completely separated, and these overlapping spectral information will seriously interfere with the classification of the network. Therefore, in [39], a spectral interclass slicing method was proposed for removing spectral redundancy information. However, the adaptation of spectral interclass slicing was still not achieved, and there are certain limitations to its generalization. Therefore, this article alleviates the deficiency of spectral redundancy information by establishing a dependence relationship between close-range and long-range spectral information. However, the receptive field of CNNs is limited by the size of the convolutional kernel, which makes it difficult to establish the long-range dependence of spectral information. As shown in Fig. 3, assuming that the band dependence relationship in the box connected by the red dashed line needs to be established, it is difficult to achieve using existing methods. Therefore, an NBR strategy is proposed in this article.

Specifically, the original bands are first grouped based on the correlation between bands. In this article, a simple and effective spectral grouping method [40], [41], [42] is adopted. As shown in Fig. 4, each yellow box is grouped into a group in different datasets. Specifically, the spectral bands of the Indian Pines (IN) dataset are grouped into three groups (1–35 as a group, 36–104 as a group, and 105–200 as a group); the spectral bands of the Salinas Valley (SV) dataset are also grouped into three groups (1–40 as a group, 41–104 as a group,

and 105–204 as a group); and the spectral bands of the Pavia University (UP) dataset are grouped into two groups (1–40 as a group and 41–104 as a group). The process of spectral correlation analysis can be expressed as

$$C(i, j) = \mathrm{Cov}(i, j)/\sqrt{\overline{\mathrm{Cov}(i, i) \cdot \mathrm{Cov}(j, j)}}. \quad (1)$$

Among them, $C(i, j)$ represents the correlation between the ith and jth bands. $\mathrm{Cov}(\cdot)$ represents the covariance operation. Subsequently, the spectrum were regrouped again within each group. Specifically, each group is once again evenly divided into B_1, B_2, and B_3. Then, nonadjacent band groups are inserted between adjacent band groups, that is, B_1 is inserted between adjacent groups B_2 and B_3. In this way, CNNs can establish the dependence of nonlocal spectral bands even through a limited receptive field. This process can be expressed as

$$B_n = \mathrm{Slice}_{-1}(x_C)\Big|_{\lceil (n-1)(b/3)\rceil}^{\lceil n(b/3)\rceil} \quad (2)$$

$$x' = \mathrm{NBR}(B_1, B_2, B_3). \quad (3)$$

Among them, $\mathrm{Slice}_{-1}(\cdot)$ represents the spectral slicing operation. x_C is the output of the correlation group. $\lceil \cdot \rceil$ is an upward rounding function, and b represents the number of spectral bands. n represents the number of groups for spectral regrouping. B_n is the result obtained by grouping. $\mathrm{NBR}(\cdot)$ represents the nonlocal band connection operation that inserts B_1 between adjacent groups B_2 and B_3.

C. Double-Pyramid Spectral–Spatial Attention

The attention mechanism is a strategy-designed inspired by human vision. The attention mechanism can enable the network to focus on important features that are beneficial for classification and suppress irrelevant features that interfere with classification. In other words, the attention mechanism can alleviate the interference of redundant information and effectively improve the classification performance of the network. In [43], an effective attention was proposed, which has achieved good classification performance. However, the computational complexity of the network is relatively high. Therefore, a DPSSA is designed in this article. As shown in Figs. 5 and 6, DPSSA consists of DPSpe_A and DPSpa_A. In general, spectral attention is first modeled by DPSpe_A, and then, spatial attention is captured by DPSpa_A. Specifically, a skip connection is adopted in DPSpe_A to reduce information loss, which is beneficial for capturing subsequent spatial attention. In addition, in order to achieve a better fusion of spectral–spatial attention, a residual structure was used between DPSpe_A and DPSpa_A. Specifically, in DPSpe_A, the key tensor K, query tensor Q, and value tensor V are obtained through a linear transformation of the input. This process can be described as

$$K = (W_K \cdot r(x_{\mathrm{in}}))^\Gamma, \quad x_{\mathrm{in}} \in \mathbb{R}^{b \times h \times w} \quad (4)$$

$$Q = W_Q \cdot r(x_{\mathrm{in}}), \quad x_{\mathrm{in}} \in \mathbb{R}^{b \times h \times w} \quad (5)$$

$$V = W_V \cdot r(x_{\mathrm{in}}), \quad x_{\mathrm{in}} \in \mathbb{R}^{b \times h \times w}. \quad (6)$$

Among them, b, h, and w represent the band, height, and width, respectively. W_K, W_Q, and W_V all represent the
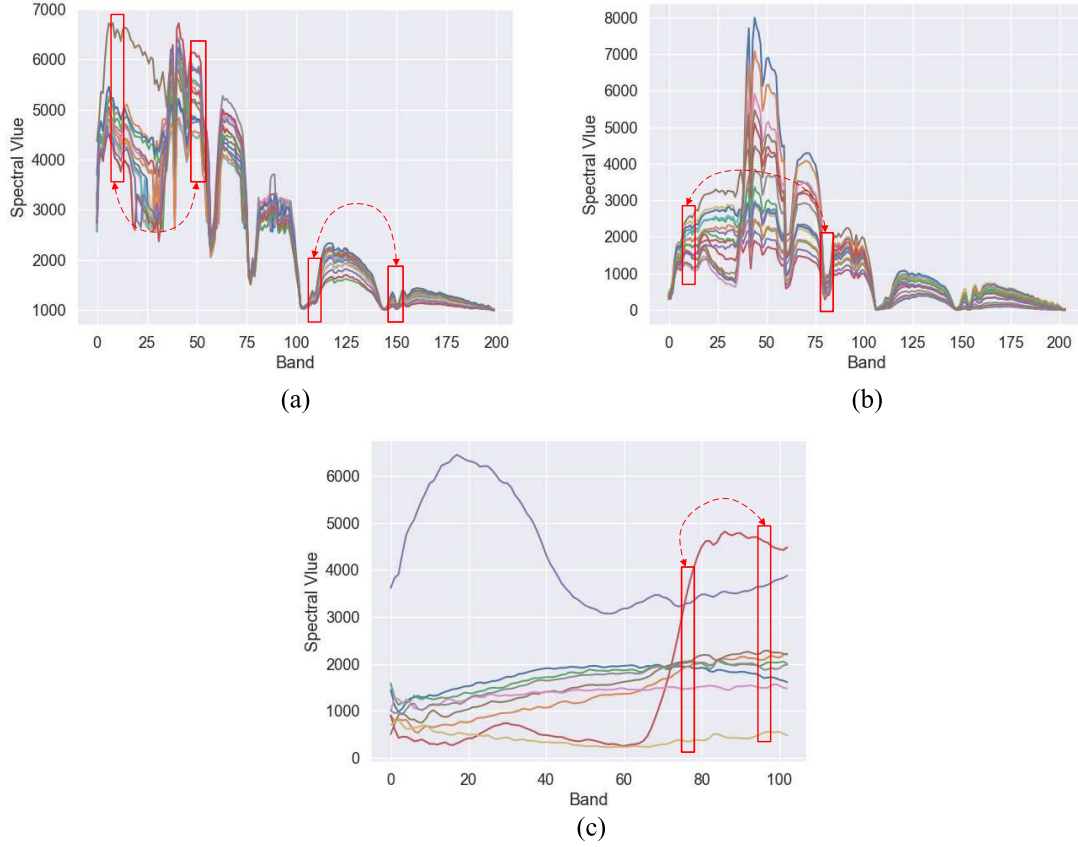
Fig. 3. Spectral curves of different datasets: (a) spectral curve of IN dataset; (b) spectral curve of SV dataset; and (c) spectral curve of UP dataset. (Among them, curves of different colors correspond to the spectra of different ground objects.)
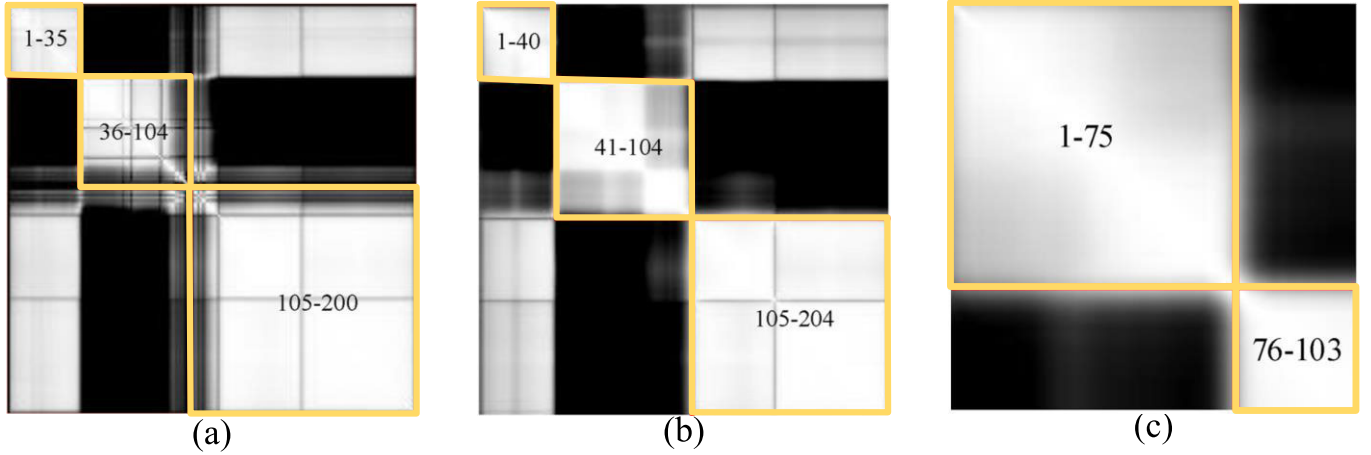

Fig. 4. Correlation analysis of spectra from different datasets: (a) IN dataset; (b) SV dataset; and (c) UP dataset. (The spectral correlation gradually increases from dark to bright.)

operation of the linear transformation layer. $r(\cdot)$ is the transformation of the spatial dimension of input x_{in} from $h \times w$ to n, that is, $n = h \times w$. Then, unlike [43], in order to reduce the computational complexity of the network, a dual pyramid is used to capture attention mask and model advanced feature V'.

Specifically, in order to avoid the loss of critical information, a multiscale pooling method is adopted for dual-pyramid pooling. This process can be described as

$$K' = P_1(K)||P_2(K)||P_4(K)||P_8(K) \tag{7}$$
$$V' = P_1(V)||P_2(V)||P_4(V)||P_8(V). \tag{8}$$

Among them, P_1, P_2, P_4, and P_8 represent the adaptive average pooling with scales 1, 2, 4, and 8, respectively. $||$ represents a connection operation. Next, K' and Q are
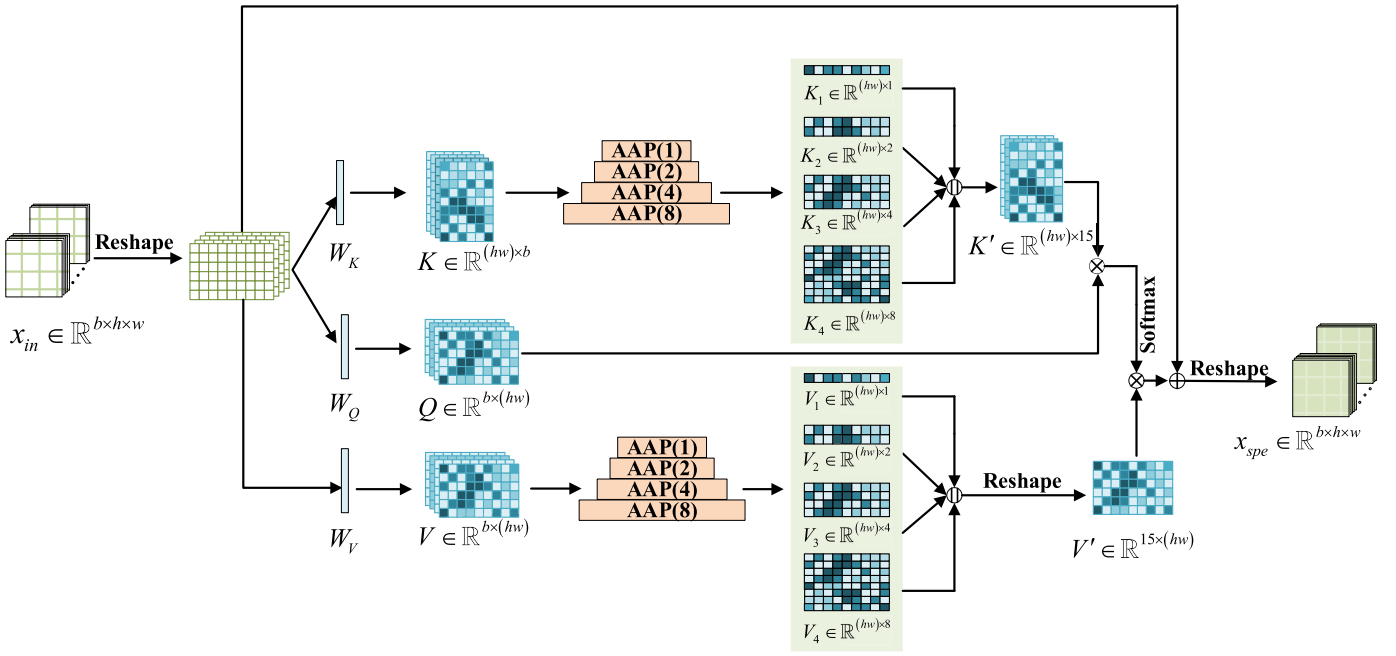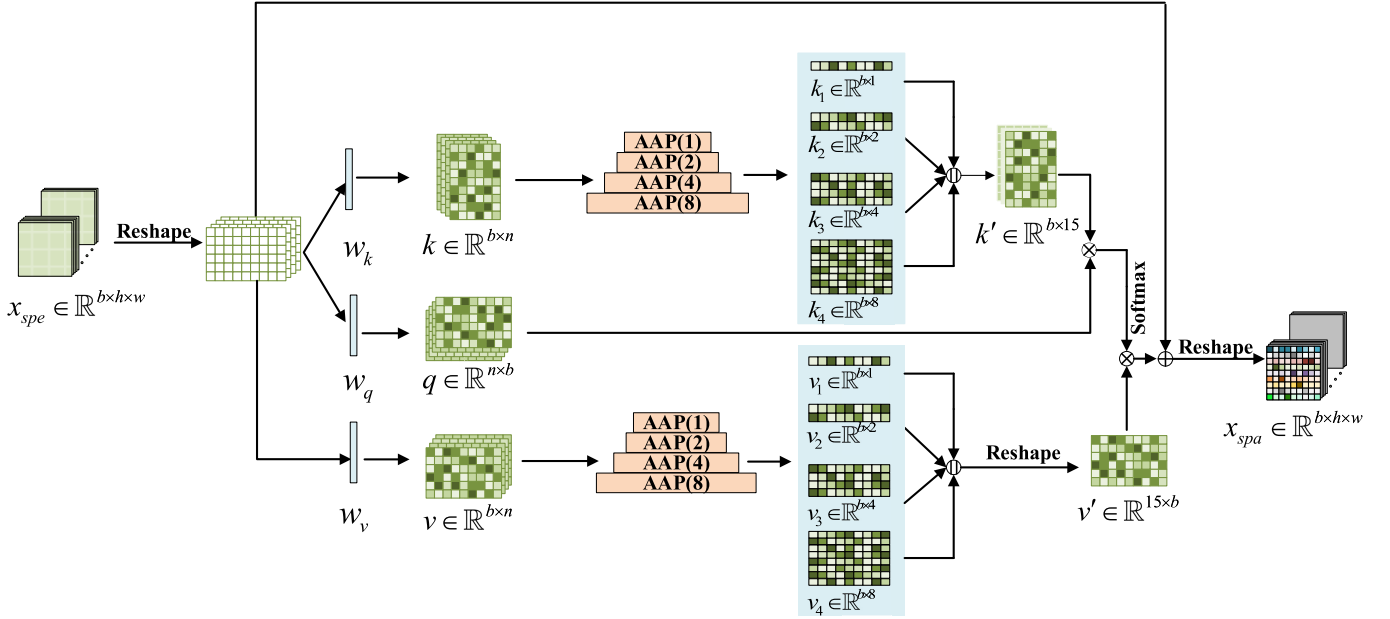
Fig. 5. Double-pyramid spectral attention.

Fig. 6. Double-pyramid spatial attention.

used to obtain spectral attention masks by point multiplication. Finally, spectral attention masks are used to weight advanced feature V'. In addition, a skip connection is used at the final stage to prevent the network from over-fitting. This process can be expressed as

$$x_{\text{spe}} = \text{relu}\big(r(x_{\text{in}}) + \text{sf}\big(K' \cdot Q\big) \cdot V'\big). \qquad (9)$$

Among them, $\text{sf}(\cdot)$ represents the softmax function. $\text{relu}(\cdot)$ is the activation function. x_{spe} is the final spectral attention obtained. In terms of network computing complexity, DPSpe_A mainly relies on the double-pyramid pooling to

reduce the computational complexity of the network. The computational complexity of DPSpe_A can be expressed as

$$O = o_1\big(b \times n^2 \times 15\big) + o_2\big(n \times b \times 15^2\big). \qquad (10)$$

The computational complexity without using double-pyramid pooling can be expressed as

$$O' = o_1\big(b^2 \times n^2\big) + o_2\big(n^3 \times b\big). \qquad (11)$$

Among them, o_1 is the computational complexity of the spectral attention mask. o_2 is the computational complexity of the spectral attention. In contrast, the computational complexity of DPSpe_A using double-pyramid pooling has been
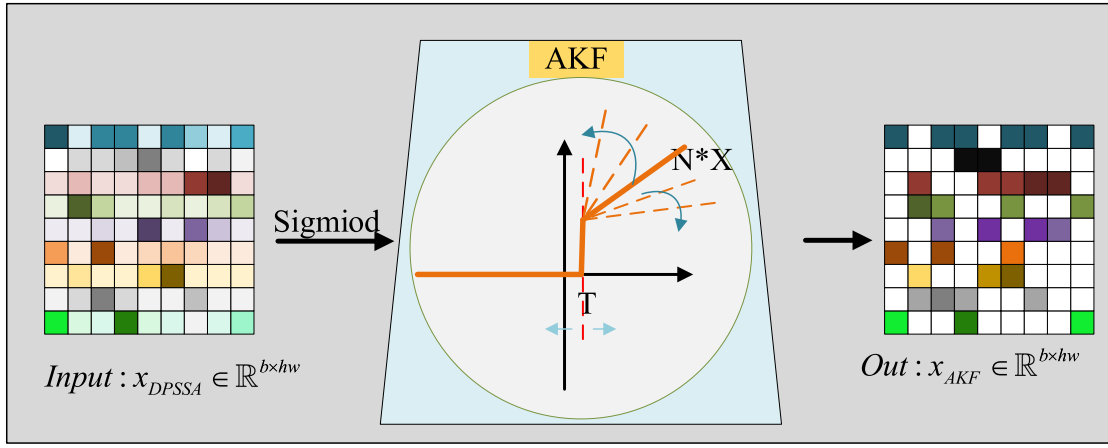
Fig. 7. Schematic of AKF.

Fig. 8. (a) OA corresponding to the use of different N and T by KF on the IN dataset. (b) Adaptive flowchart of AKF on IN dataset.

significantly reduced. Specifically, the computational complexity of attention masks has been reduced by $b/15$ times, and the complexity of attention has been reduced by $n^2/15^2$ times. In this article, in order to simplify the network structure, the structures of DPSpa_A and DPSpe_A are similar. As shown in Figs. 4 and 5, the difference is that the double pyramid pooling layer in DPSpa_A acts on the spatial dimension, while the double pyramid pooling layer in DPSpe_A acts on the spectral dimension. Therefore, this article will not repeat the description of DPSpa_A.

D. Adaptive Knowledge Filter

In order to alleviate the interference of redundant information on the network, attention mechanisms have provided effective solutions. However, the attention mechanism relies on the network's feature extraction ability, and redundant information cannot be directly removed. Recently, a feature filter [44] has been used to eliminate redundant information. Although the feature filter proposed in [44] has achieved some achievements in the application of HSIC, this method has not achieved adaptation. This makes the feature filter require manual adjustment of parameters to adapt to different datasets, and it is also difficult to integrate into other networks. In addition, the feature filter changes all feature values greater than the threshold to 1, which increases the risk of network interference from redundant information that has not been fully filtered.

In this article, an AKF is proposed to further alleviate the interference of redundant information on the network. As shown in Fig. 7, the threshold T and gain value N are first set for the proposed knowledge filter (KF). Specifically, the feature values of the input filter are represented as x_{DPSSA}. First, the sigmoid function is used to normalize x_{DPSSA} to obtain feature X, which is then input into the KF. When the feature values of the input KF are greater than T, the input feature values will be augmented (i.e., the feature values X will become $N * X$). On the contrary, when the input feature values of the KF are less than T, the input feature values will be set to 0. This process can be described as

$$X = \text{sigmiod}(x_{\text{DPSSA}}), \quad x_{\text{DPSSA}} \in \mathbb{R}^{b \times hw} \quad (12)$$

$$X = \begin{cases} N * X, & X \geq T \\ 0, & X < T. \end{cases} \quad (13)$$

Subsequently, in order to improve the generalization of the network and enable KFs to be widely applied in HSIC, an AKF is proposed in this article. The adaptive process of AKF is shown in Algorithm 1.

Algorithm 1 The Adaptive Process of AKF

Input: Input $x \in \mathbb{R}^{h \times w \times b}$.

Output: parameters of the optimal model.

1. Initialization, $Flag = 0$, $NFlag = 1$, $TFlag = 0$, $BOA = 0$, $ROA = 0$, $S = 1$, $s = 0.1$.
2. **for** i=1 to epoch **do**
3. Perform training on the FCAN_AKF model. Update and save training parameters.
4. Perform validation of the FCAN_AKF model. Calculate the loss value and save the ROA.
5. Determine if the loss value has decreased. If the loss value decreases, make $Flag = 0$ and perform 2. Otherwise, $Flag = Flag + 1$ is performed.
6. Determine if $Flag$ is equal to 10. If $Flag = 10$, then $Flag = 0$ will be performed. Otherwise, 2 is performed.
7. Determine if $NFlag$ is equal to 1. If $NFlag = 1$, then 8 will be performed. Otherwise, 9 is performed.
8. Determine if ROA is greater than BOA. If $ROA > BOA$, then $BOA = ROA$ will be performed. In addition, make $NFlag = 0$, $TFlag = 1$, $N = N + S$ and perform 2. Otherwise, make $NFlag = 0$, $TFlag = 1$, $N = N - 2S$ and perform 2.
9. Determine if $TFlag$ is equal to 1. If $TFlag = 1$, then 10 will be performed. Otherwise, 2 is performed.
10. Determine if ROA is greater than BOA. If $ROA > BOA$, then $BOA = ROA$ will be performed. In addition, make $TFlag = 0$, $NFlag = 1$, $T = T + s$ and perform 2. Otherwise, make $TFlag = 0$, $NFlag = 1$, $T = T - 2s$ and perform 2.

    end for

In Algorithm 1, Flag, NFlag, and TFlag represent, in turn, the flag for performing AKF, the flag for updating N, and the flag for updating T. When Flag = 10, the adaptation of the KF is started. When NFlag = 1, the update of gain value N is performed. When TFlag = 1, the update of the threshold is performed. BOA and ROA are the best prediction accuracy and current prediction accuracy of the model in sequence. S and s are the update steps of N value and T value, respectively. Epoch is the maximum number of training iterations for the network. In general, the adaptation of AKF involves cross-updating N and T through network training iterations to adaptively filter out redundant information and enhance important information. Specifically, the network parameters are first saved through network training and then used for validation. During the validation phase, the loss value of the current network will be calculated, and the prediction accuracy of the current network will be saved. Then, the network will be judged whether to preconvergence (verifying that the loss continuously increases ten times, i.e., Flag = 10). When the network reaches preconvergence, the N and T values of AKF will be cross-updated. This process is repeated until the network training is completed. Specifically, in order to avoid local optima in the classification performance of the network, a method of cross-updating N and T is designed. In addition,

the update step size of N and T values can be adjusted in AKF.

As shown in Fig. 8(b), the adaptive update process of N and T is demonstrated on the IN dataset. Among them, the red, orange, and purple guidelines represent the adaptive process of the network under different initial N and T values. As shown in Fig. 8(b), regardless of how the initial values of N and T are set, the optimal classification performance of the network can ultimately be obtained through AKF adaptation. Taking the red guideline as an example, the classification accuracy corresponding to the red dots is the classification accuracy corresponding to the initial N and T (i.e., the classification accuracy corresponding to the network when $N = 1$ and $T = 0.1$). Then, the optimal classification performance of the network is obtained through iterative training of the network and adaptive filtering of redundant information through cross-updating N and T.

In short, the interference of redundant information on the network can be effectively alleviated by the proposed AKF. In addition, compared to the feature filter proposed in [44], the AKF proposed in this article can be implemented adaptively. And in AKF, the linear gain method is adopted to enhance features larger than the threshold, which preserves the differences between the obtained features to further remove redundant information in the next adaptive filtering.

III. EXPERIMENTATION AND ANALYSIS

In order to verify the effectiveness of the FCAN_AKF, experiments and analyses were conducted on the proposed method in this section. First, three datasets are presented in detail. Then, the details of the hyperparameter setting of the network are given. Subsequently, the ablation experiment was used to analyze the effectiveness of the proposed module in this article. In addition, the classification performance of the proposed network has been analyzed in detail. Finally, this article proves that the FCAN_AKF is more competitive compared to some state-of-the-art methods. In particular, in order to avoid the contingency of the experiment, the results of all experiments are the average results of ten repeated experiments. And all experiments were conducted in the same experimental environment. Specifically, the experiment was equipped with NVIDIA GeForce RTX 3070 and the compilation software was PyCharm 2020. The running environment of the code is in PyTorch 1.10.0 and Python 3.7.12.

A. HSI Dataset and Evaluation Indicators for Classification Performance

This article verifies the classification performance of the FCAN_AKF on three challenging datasets, including IN, SV, and UP. IN has 200 consecutive spectral bands, 16 classes, and 10 249 labeled pixels. SV has 204 consecutive bands and also includes 16 classes, covering 54 129 pixels. UP has 104 bands, and it includes nine classes. The number of pixels covered by its ground objects is 42 776. The detailed information of the three datasets is shown in Figs. 9–11. In this article, a unified proportion of training and testing samples is used in all experiments. Specifically, 3% of the training samples

No.	Legend	Name	Sample	train sample	validation sample
1		Alfafa	46	3	43
2		Corn–n	1428	42	1386
3		Corn–m	830	24	806
4		Corn	237	7	230
5		Grass–p	483	14	469
6		Grass–t	730	21	709
7		Grass–p–m	28	3	25
8		Hay-w	478	14	464
9		Oats	20	3	17
10		Soybean-n	972	29	943
11		Soybean-m	2455	73	2382
12		Soybean-c	593	17	576
13		Wheat	205	6	199
14		Woods	1265	37	1228
15		Buildings-G-T	386	11	375
16		Stone-S-T	93	3	90
TOTAL			10249	307	9942

Ground truth

Fig. 9. Details of the IN.

No.	Legend	Name	Sample	train sample	test sample
1		weeds_1	2009	20	1989
2		weeds_2	3726	37	3689
3		Fallow	1976	19	1957
4		Fallow-r-p	1394	13	1381
5		Fallow-s	2678	26	2652
6		Stubble	3959	39	3920
7		Celery	3579	35	3544
8		Grapes-u	11271	112	11159
9		Soil-v-y-d	6203	62	6141
10		C-s-g-weeds	3278	32	3246
11		L-r-4wk	1068	10	1058
12		L-r-5wk	1927	19	1908
13		L-r-6wk	916	9	907
14		L-r-7wk	1070	10	1060
15		VIN-yard-u	7268	72	7196
16		VIN-yard-v-t	1807	18	1789
TOTAL			54129	533	53596

Ground truth

Fig. 10. Details of the SV.

were used on the IN. The 1% of the training samples were used on the SV and UP. In addition, in order to quantitatively evaluate the classification performance of the network, three important evaluation indicators are used in this article. This includes overall classification accuracy (OA), average accuracy (AA), and KAPPA coefficient.

No.	Legend	Name	Sample	train sample	test sample
1		Asphalt	6631	66	6565
2		Meadows	18649	186	18463
3		Gravel	2099	20	2079
4		Trees	3064	30	3034
5		Painted m s	1345	13	1332
6		B Soil	5029	50	4979
7		Bitumen	1330	13	1317
8		S-B Bricks	3682	36	3646
9		Shadows	947	9	938
TOTAL			42776	423	42353

Ground truth
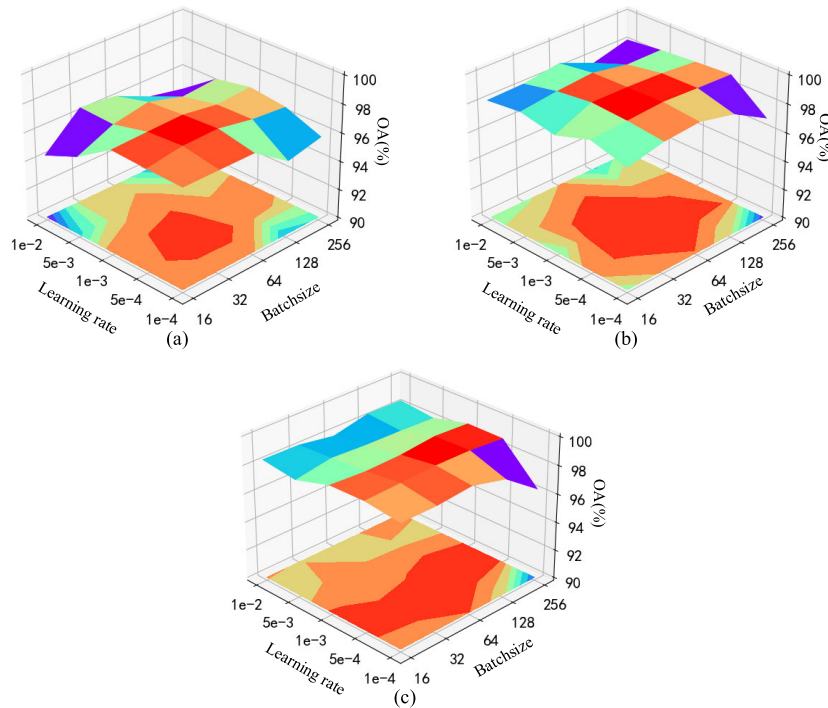
Fig. 11. Details of the UP.

Fig. 12. Impact of different training batches on classification performance of networks under different learning rates: (a) experimental results on the IN dataset; (b) experimental results on the SV dataset; and (c) experimental results on the UP dataset.

B. Hyperparameter Setting

In CNNs, the influence of hyperparameter on model training cannot be ignored. In order to obtain the best classification performance of the network, it is necessary to set an appropriate hyperparameter for the network. First, the epoch of FCAN_AKF is set to 400. The impact of learning rate and training batch on the classification performance of the proposed network on different datasets is shown in Fig. 12. As shown in Fig. 12(a), on the IN, when the learning rate of the FCAN_AKF is determined, the classification performance of the network first increases and then decreases as the batch size of the network input increases. And when the input batch size is 64, the best classification performance is achieved. Similarly, when the input batch size is determined, the classification performance of the network first increases and then decreases as the learning rate increases. And when the learning rate is $5e^{-4}$, the best network performance is achieved. As shown in Fig. 12(a) and (b), the impact of learning rate and training batch size on the classification performance of the proposed network on the SV and UP datasets is similar to that on the IN dataset. Therefore, the learning rate and input batch size of FCAN_AKF are set to $5e^{-4}$ and 64, respectively.

TABLE I
ABLATION EXPERIMENT ($\sqrt{}$ INDICATES WITH CORRESPONDING MODULE, AND — INDICATES WITHOUT CORRESPONDING MODULE)

	Number	1	2	3	4	5	6	7	8
Method	NBR	—	—	—	$\sqrt{}$	—	$\sqrt{}$	$\sqrt{}$	$\sqrt{}$
	AKF	—	—	$\sqrt{}$	—	$\sqrt{}$	—	$\sqrt{}$	$\sqrt{}$
	DPSSA	—	$\sqrt{}$	—	—	$\sqrt{}$	$\sqrt{}$	—	$\sqrt{}$
	Basic	$\sqrt{}$	$\sqrt{}$	$\sqrt{}$	$\sqrt{}$	$\sqrt{}$	$\sqrt{}$	$\sqrt{}$	$\sqrt{}$
Datasets	IN	96.04	96.55	96.70	96.38	96.99	96.85	96.89	97.41
	SV	98.01	98.46	98.63	98.38	98.88	98.79	98.82	99.09
	UP	98.23	98.54	98.69	98.49	98.97	98.81	98.91	99.22

1. FCAN_AKF (basic network, i.e. without NBR, AKF, and DPSSA)

2. FCAN_AKF(only with DPSSA module)

3. FCAN_AKF(only with AKF module)

4. FCAN_AKF(only with NBR strategy)

5. FCAN_AKF(with DPSSA and AKF)

6. FCAN_AKF(with NBR and DPSSA)

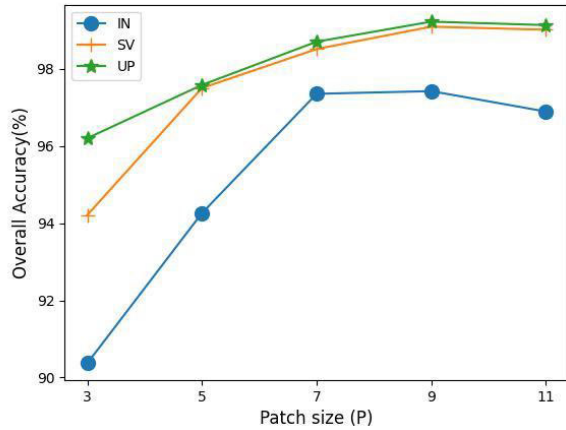7. FCAN_AKF(with NBR and AKF)

8. Complete FCAN_AKF

Fig. 13. Impact of the size of network input patch. (The size of the patch is $P \times P$.)

In addition, the impact of the size of input patch on the classification performance of CNNs cannot be ignored. Therefore, in Fig. 13, the impact of input patch size on FCAN_AKF classification performance was explored for different datasets. In general, on the three datasets, the classification performance of the network first increases and then decreases as the input patch size increases. And when the size of the patch is 9×9, the optimal classification performance is obtained by the proposed network. Therefore, the input patch size of FCAN_AKF is set to 9×9.

C. Effectiveness Analysis of the Proposed Modules

Some ablation experiments were conducted by the proposed modules. As shown in Table I, eight sets of experiments are conducted on each dataset. First, the experimental results of experiment 1 FCAN_AKF (basic network, i.e., without NBR, AKF, and DPSSA) and experiment 2 FCAN_AKF (only with DPSSA module) were compared, and it was found that the classification accuracy of the network can be effectively improved by DPSSA on three different datasets. Specifically, on the IN dataset, when DPSSA is used, the classification accuracy of the network is improved by 0.5% compared to when DPSSA is not used. Similarly, on the SV dataset, OA improved by 0.45%. On the UP dataset, OA improved by 0.31%. The classification performance of networks can be effectively improved by DPSSA because it can enhance important features through attention and effectively suppress unimportant features. In addition, DPSSA reduces information loss through multiscale pyramid pooling. Subsequently, experiment 1 FCAN_AKF (basic network, i.e., without NBR, AKF, and DPSSA) and experiment 4 FCAN_AKF (only with NBR strategy) were compared, and the effectiveness of NBR strategy was also verified. Obviously, on the IN dataset, compared to FCAN_AKF without NBR strategy, the OA of FCAN_AKF with NBR strategy increased by 0.34%. Similarly, on the other two datasets, compared to FCAN_AKF without NBR strategy, FCAN_AKF with NBR strategy showed varying degrees of improvement in classification accuracy. This is because NBR can enable the network to capture nonlocal spectral features by regrouping the original spectral, thereby establishing interdependence between close-range spectral information and long-range spectral information. Moreover, the nonlocal features after spectral regrouping are combined with the local features of the original HSIs, achieving feature fusion and complementarity. Therefore, the classification performance of the network can be effectively improved. Finally, experiment 1 FCAN_AKF (basic network, i.e., without NBR, AKF, and DPSSA) was compared with experiment 3 FCAN_AKF (only with AKF module), and the results showed that compared to FCAN_AKF without AKF, FCAN_AKF with AKF showed significant improvement in classification performance on all three datasets. This is because AKF can adaptively remove redundant information and gain important feature information.

In addition, to verify whether NBR, AKF, and DPSSA will interfere with each other in FCAN_AKF, experiment 5 FCAN_AKF (with DPSSA and AKF) and
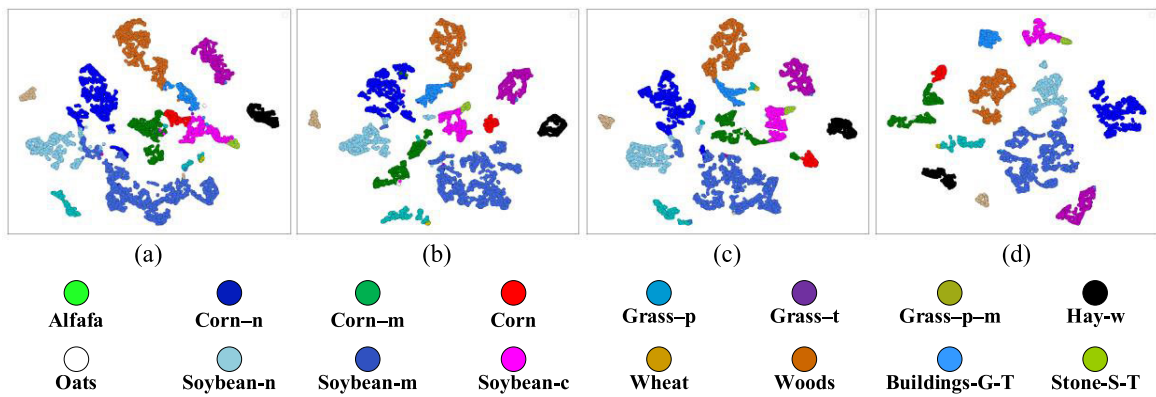
| Alfafa | Corn–n | Corn–m | Corn | Grass–p | Grass–t | Grass–p–m | Hay-w |
| Oats | Soybean-n | Soybean-m | Soybean-c | Wheat | Woods | Buildings-G-T | Stone-S-T |

Fig. 14. Visualization of classification results for different strategies on the IN dataset: (a) FCAN_AKF (basic network, i.e., without NBR, AKF, and DPSSA); (b) FCAN_AKF (only with DPSSA module); (c) FCAN_AKF (with DPSSA and AKF); and (d) complete FCAN_AKF.

| weeds_1 | weeds_2 | Fallow | Fallow-r-p | Fallow-s | Stubble | Celery | Grapes-u |
| Soil-v-y-d | C-s-g-weeds | L-r-4wk | L-r-5wk | L-r-6wk | L-r-7wk | VIN-yard-u | VIN-yard-v-t |

Fig. 15. Visualization of classification results for different strategies on the SV dataset: (a) FCAN_AKF (basic network, i.e., without NBR, AKF, and DPSSA); (b) FCAN_AKF (only with DPSSA module); (c) FCAN_AKF (with DPSSA and AKF); and (d) complete FCAN_AKF.
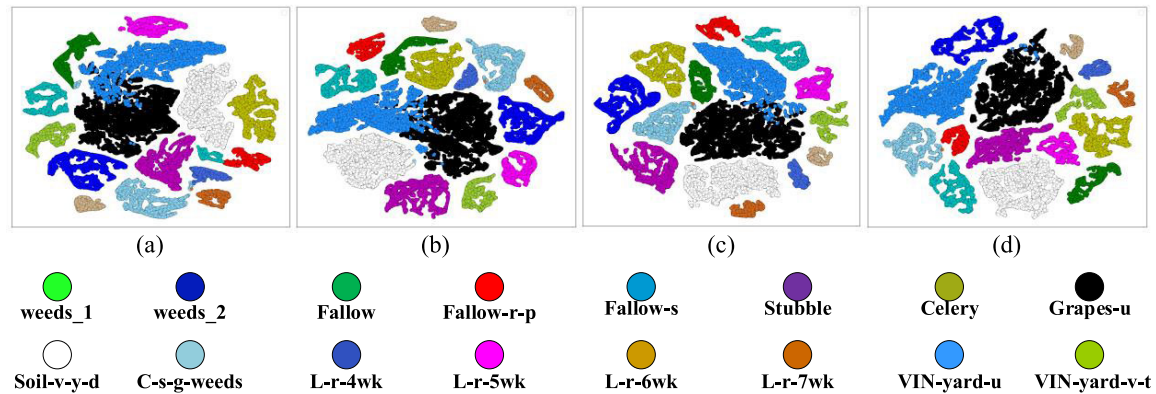

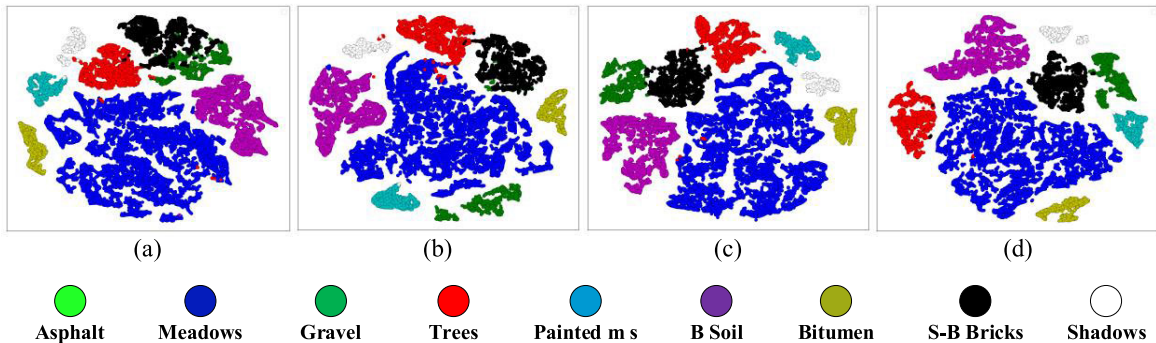| Asphalt | Meadows | Gravel | Trees | Painted m s | B Soil | Bitumen | S-B Bricks | Shadows |

Fig. 16. Visualization of classification results for different strategies on the UP dataset: (a) FCAN_AKF (basic network, i.e., without NBR, AKF, and DPSSA); (b) FCAN_AKF (only with DPSSA module); (c) FCAN_AKF (with DPSSA and AKF); and (d) complete FCAN_AKF.

experiment 8 complete FCAN_AKF were compared, experiment 6 FCAN_AKF (with NBR and DPSSA) and experiment 8 complete FCAN_AKF were compared, and experiment 7 FCAN_AKF (with NBR and AKF) and experiment 8 complete FCAN_AKF were compared, respectively. Obviously, NBR, AKF, and DPSSA do not interfere with each other in FCAN_AKF, and the classification accuracy of the network can be effectively improved in any situation.

In order to more intuitively analyze the impact of the proposed modules on network performance, this article conducts incremental analysis of the proposed modules on each dataset step by step. Specifically, the visualization of classification results using different strategies on the IN dataset is shown in Fig. 14. Fig. 14(a) shows a visualization of the classification results of the basic network (i.e., FCAN_AKF only removes NBR, AKF, and DPSSA modules). Fig. 14(b) shows a visualization of the classification results obtained by adding the DPSSA module to the basic network. Obviously, compared to Fig. 14(a), Fig. 14(b) shows more clustering among the same classes and more dispersion among different classes. This indicates that the classification performance of the network has been effectively improved by the DPSSA module. Based

TABLE II
CLASSIFICATION RESULTS ON IN

Methods	DBDA	DBMA	HPDM-SPRN	SSTN	A2S2KResNet	HResNetAM	FECNet	FCAN_AKF
1	78.69(0.1420)	83.74(0.1029)	80.14(0.3176)	90.23(0.1122)	87.89(0.1220)	96.61(0.0324)	92.31(0.1273)	**99.29(0.0107)**
2	90.63(0.0413)	92.58(0.0315)	96.24(0.0157)	96.29(0.0098)	93.30(0.0319)	95.32(0.0184)	95.99(0.0226)	**98.34(0.0035)**
3	89.88(0.0721)	92.10(0.0576)	98.23(0.0169)	95.47(0.0208)	94.67(0.0212)	95.38(0.0266)	95.15(0.0345)	**98.39(0.0043)**
4	87.03(0.0802)	90.37(0.0563)	85.50(0.1272)	**95.28(0.0255)**	94.88(0.0297)	94.45(0.0474)	92.87(0.0610)	93.23(0.0268)
5	98.41(0.0206)	94.37(0.0444)	94.72(0.0224)	91.88(0.0182)	97.75(0.0197)	**98.61(0.0155)**	97.90(0.0165)	96.59(0.0152)
6	96.10(0.0389)	97.41(0.0208)	99.11(0.0026)	98.21(0.0091)	96.51(0.0214)	98.02(0.0250)	96.99(0.1942)	**99.21(0.0030)**
7	64.78(0.1997)	56.74(0.1524)	55.56(0.4569)	**84.07(0.2121)**	74.87(0.2245)	71.77(0.2023)	74.85(0.1865)	78.68(0.0633)
8	99.75(0.0054)	99.78(0.0048)	99.96(0.0009)	100.0(0.0000)	99.91(0.0020)	99.93(0.0019)	99.95(0.0013)	**100.0(0.0000)**
9	50.65(0.1150)	58.45(0.1410)	**87.25(0.2950)**	72.63(0.2035)	59.61(0.1705)	82.30(0.1701)	66.22(0.1767)	81.90(0.0673)
10	89.40(0.0368)	88.14(0.0438)	93.07(0.0295)	92.37(0.0344)	90.25(0.0445)	90.90(0.0619)	91.16(0.0397)	**96.59(0.0087)**
11	92.34(0.0247)	92.65(0.0268)	97.01(0.0056)	96.50(0.0173)	96.71(0.0108)	97.10(0.0155)	97.19(0.0145)	**97.20(0.0044)**
12	85.65(0.0818)	85.89(0.0754)	**98.02(0.0149)**	95.09(0.0154)	93.97(0.0367)	93.44(0.0591)	92.75(0.0468)	94.95(0.0212)
13	98.54(0.0272)	95.58(0.0754)	99.06(0.0232)	98.73(0.0120)	97.53(0.0269)	98.39(0.0337)	96.52(0.0433)	**99.48(0.0065)**
14	97.04(0.0136)	96.16(0.0222)	99.25(0.0075)	99.22(0.0048)	97.72(0.0203)	97.83(0.0161)	98.25(0.0145)	**99.54(0.0027)**
15	86.69(0.0521)	87.20(0.0524)	91.23(0.0841)	92.54(0.0588)	93.30(0.0512)	**95.25(0.0333)**	92.50(0.0449)	93.60(0.0316)
16	92.60(0.0754)	83.29(0.2392)	96.73(0.0488)	91.33(0.0979)	90.84(0.0576)	93.29(0.0589)	90.55(0.0815)	**99.64(0.0076)**
OA	91.87(0.0169)	91.76(0.0228)	96.72(0.0052)	96.03(0.0058)	95.02(0.0091)	95.88(0.0131)	95.60(0.0083)	**97.41(0.0018)**
AA	88.8(0.02261)	87.15(0.0284)	92.02(0.0591)	93.11(0.0218)	91.23(0.0210)	93.67(0.0152)	91.95(0.0218)	**94.17(0.0062)**
KAPPA	92.25(0.0192)	90.62(0.0255)	96.25(0.0059)	95.47(0.0067)	94.33(0.0104)	95.31(0.0148)	94.99(0.0095)	**97.05(0.0020)**
Params	606.906k	609.791k	205.396k	741.492k	373.184k	65.866k	317.610k	**59.382k**
Runtime	601.2s	660.3s	**79.4s**	1277.5s	1307.4s	262.3s	573.7s	556.3s

on Fig. 14(b), Fig. 14(c) has added AKF. Similarly, compared to Fig. 14(b), the classification performance of the network has once again been improved. Finally, Fig. 14(d) shows a visualization of the classification results obtained from the complete FCAN_AKF network. Compared with the previous strategies, the optimal classification performance is achieved by the complete FCAN_AKF. In addition, as shown in Figs. 15 and 16, the same conclusions can also be obtained on the SV dataset and the UP dataset. This proves that the three proposed modules do not interfere with each other, and the classification performance of the network shows an incremental improvement with their addition.

In addition, in order to reduce the parameter quantity of FCAN_AKF, DSC is introduced into FCAN_AKF. In order to verify the impact of DSC on the number of network parameters, some ablation experiments were carried out to evaluate the parameter quantity of FCAN_AKF with and without DSC. The experimental results are shown in Fig. 17. Obviously, on all these datasets, the parameter quantity of the network can be significantly reduced by DSC, which proves the effectiveness of the designed lightweight network.

D. Analysis of Classification Performance of FCAN_AKF

In this section, the classification performance of the proposed FCAN_AKF network was analyzed. As shown in Fig. 18, in order to analyze the classification performance of each class, the confusion matrix of FCAN_AKF on three
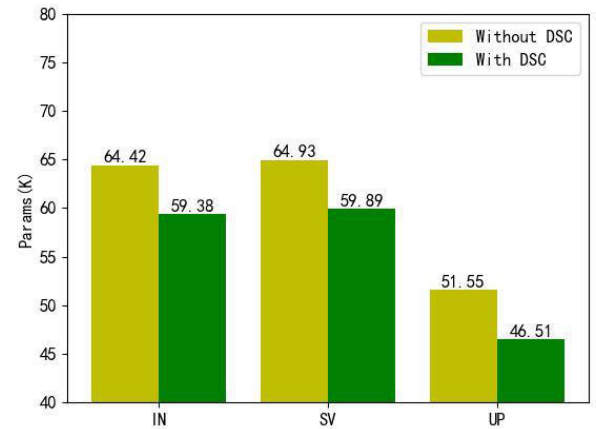

Fig. 17. Impact of DSC on network parameter quantity.

datasets is given here. In Fig. 18, the real labels are represented by the horizontal axis, and the predicted labels are represented by the vertical axis. In addition, the diagonal represents that the predicted labels are the same as the real labels, which means that the network predicts accurate labels. In general, all three challenging datasets can be effectively classified by FCAN_AKF. On the one hand, it indicates that FCAN_AKF has significant classification performance. On the other hand, different datasets can be adapted by FCAN_AKF, indicating that FCAN_AKF has excellent generalization ability. This is
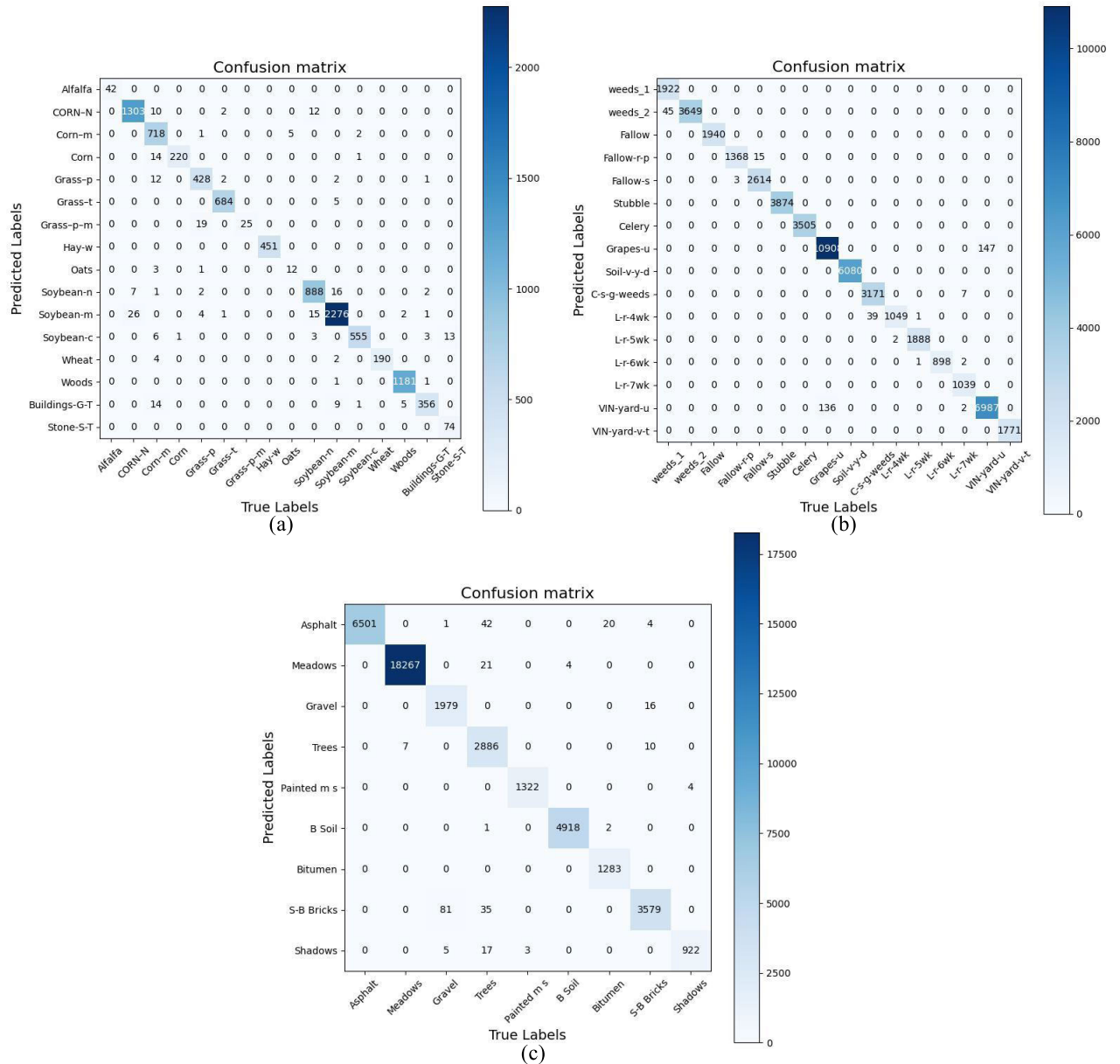
Fig. 18. Confusion matrix obtained by FCAN_AKF on different datasets: (a) confusion matrix of IN dataset; (b) confusion matrix of SV dataset; and (c) confusion matrix of the UP dataset.

because the proposed method establishes the interaction of long-range spectral information and achieves complementarity between local and nonlocal features. In addition, the interference of redundant information is also effectively alleviated by FCAN_AKF. However, a small amount of misclassification is still inevitable. And these misclassification situations almost all occur between adjacent class boundaries. This is also what we need to focus on in the future work.

E. Analysis of Classification Performance of FCAN_AKF

In order to further verify the effectiveness of the proposed network, this section will include the proposed FCAN_AKF that was compared with seven CNN-based HSIC methods. These seven methods include: double-branch multi-attention (DBMA) [26], DBDA [27], spectral–spatial transformer network (SSTN) [28], hierarchical residual

network with attention mechanism (HResNetAM) [29], homogeneous pixel detection module-spectral partitioning residual network (HPDM-SPRN) [45], attention-based adaptive spectral–spatial kernel ResNet (A2S2KResNet) [46], and feedback expansion convolution network (FECNet) [47]. The classification results and parameter quantities of different methods on three datasets are shown in Tables II–IV.

First, the best classification performance can be achieved by the proposed FCAN_AKF on all three datasets. Moreover, in terms of the overall parameter quantity of the network, FCAN_AKF also has significant advantages compared to other methods. Specifically, the classification results and parameter quantities of all methods on the IN dataset are presented in Table II. From the classification results, compared to other methods, the proposed FCAN_AKF has significant advantages in OA, AA, and KAPPA coefficients. Especially for OA and
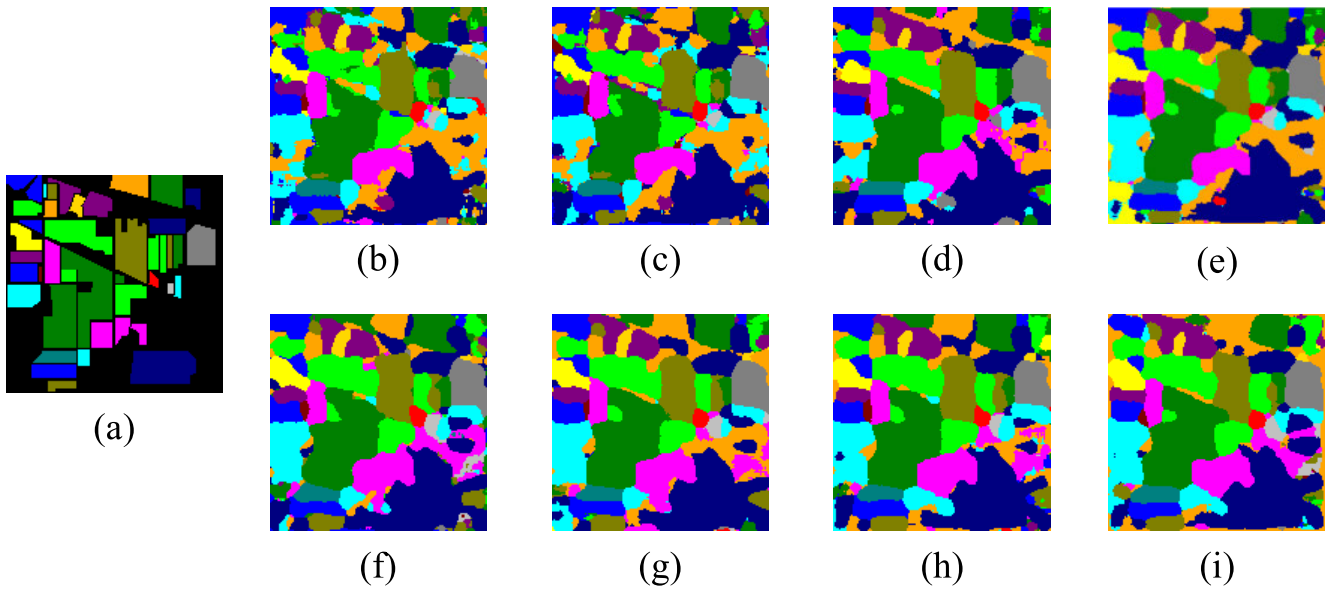
Fig. 19. Classification maps using different methods on the IN dataset: (a) real map; (b) DBMA; (c) DBDA; (d) HPDM-SPRN; (e) SSTN; (f) A2S2KResNet; (g) HResNetAM; (h) FECNet; and (i) FCAN_AKF.
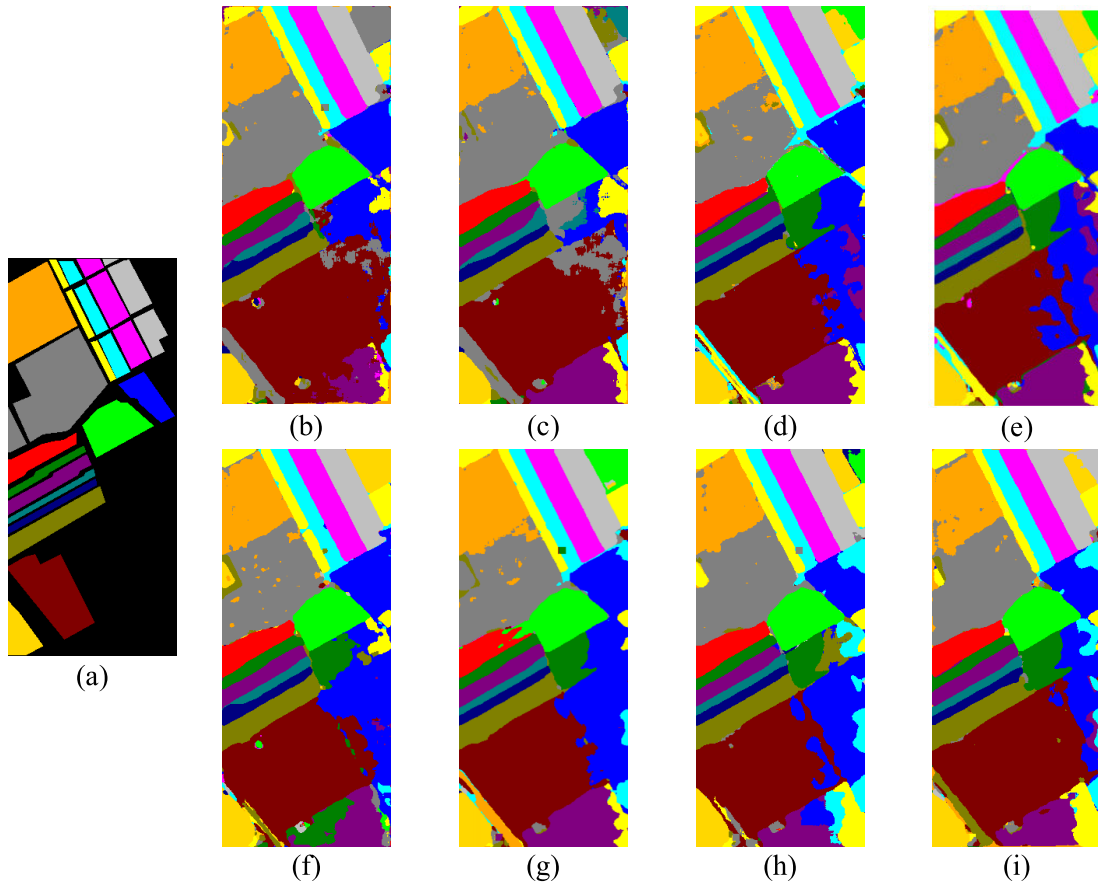

Fig. 20. Classification maps using different methods on the SV dataset: (a) real map; (b) DBMA; (c) DBDA; (d) HPDM-SPRN; (e) SSTN; (f) A2S2KResNet; (g) HResNetAM; (h) FECNet; and (i) FCAN_AKF.

KAPPA coefficients, FCAN_AKF is 1%–5% higher than other methods. This not only indicates that the overall classification performance of the proposed method is significant, but also indicates that FCAN_AKF can classify each class in a balanced manner, with good classification consistency. On the one hand, it benefits from the fusion and complementarity of local and nonlocal features. On the other hand, with the help of DPSSA and AKF, the redundant information
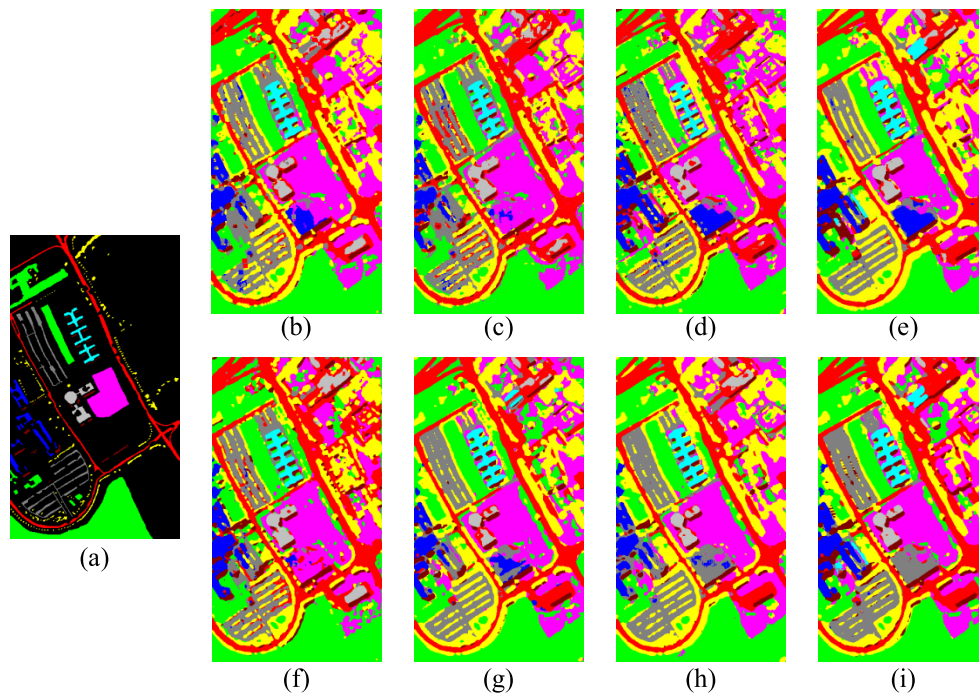
Fig. 21. Classification maps using different methods on the UP dataset: (a) real map; (b) DBMA; (c) DBDA; (d) HPDM-SPRN; (e) SSTN; (f) A2S2KResNet; (g) HResNetAM; (h) FECNet; and (i) FCAN_AKF.
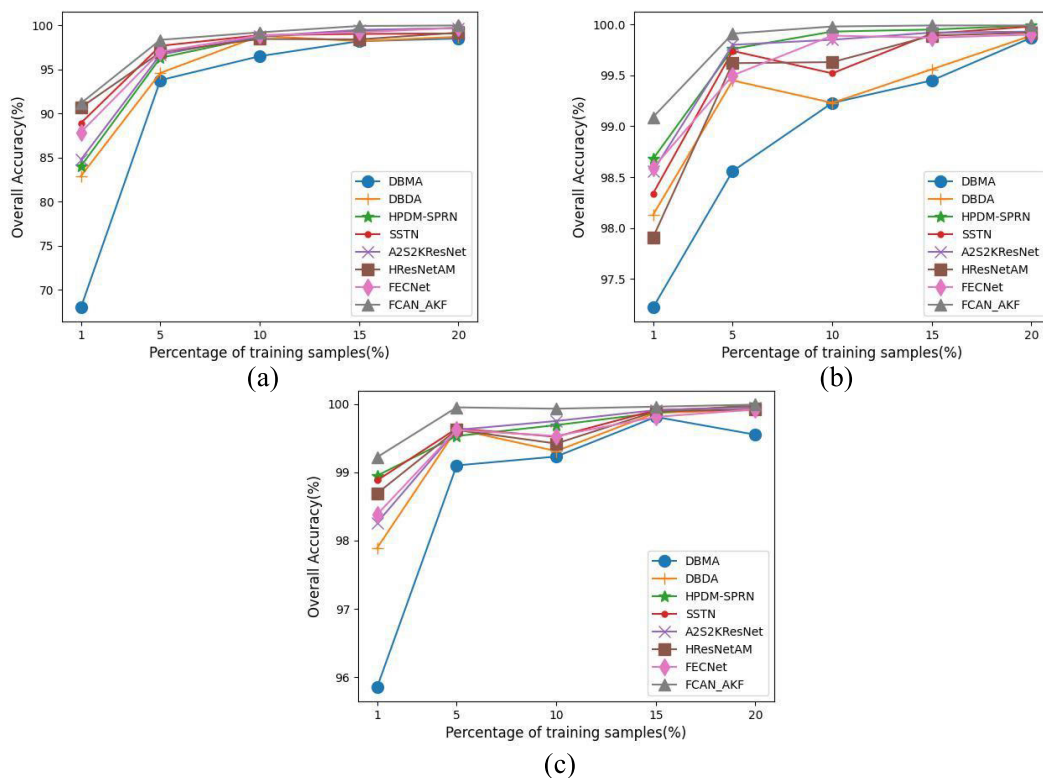

Fig. 22. Classification accuracy of all methods under different training samples: (a) IN; (b) SV; and (c) UP.

of interference classification can be effectively removed by FCAN_AKF. From the overall parameter quantity of the network, compared to other methods, the proposed method has also significant advantages on the IN dataset. Specifically, the proposed FCAN_AKF has only 59.382k parameters, which

is approximately 6k–700k lower than other methods. This is due to the simple network architecture design of FCAN_AKF, and additional parameters will not be introduced. Moreover, a DSC is used by FCAN_AKF when extracting features, which significantly reduces the number of network parameters

TABLE III
CLASSIFICATION RESULTS ON SV

Methods	DBDA	DBMA	HPDM-SPRN	SSTN	A2S2KResNet	HResNetAM	FECNet	FCAN_AKF
1	99.91(0.0017)	99.99(0.0001)	100.0(0.0000)	99.92(0.0018)	100.0(0.0000)	100.0(0.0000)	100.0(0.0000)	**100.0(0.0000)**
2	99.76(0.0039)	99.95(0.0009)	99.68(0.0003)	99.78(0.0002)	99.78(0.0004)	99.94(0.0012)	99.96(0.0005)	**99.96(0.0009)**
3	98.42(0.0279)	98.56(0.0290)	99.69(0.0016)	99.27(0.0138)	99.59(0.0041)	99.15(0.0114)	98.27(0.0278)	**99.74(0.0029)**
4	96.86(0.0289)	95.52(0.0469)	**99.34(0.0069)**	99.28(0.0043)	97.64(0.0225)	98.39(0.0128)	97.33(0.0207)	99.19(0.0016)
5	97.25(0.0347)	99.07(0.0066)	99.34(0.0053)	98.30(0.0101)	99.80(0.0020)	99.44(0.0047)	99.66(0.0059)	**99.87(0.0005)**
6	99.28(0.0134)	99.39(0.0130)	99.98(0.0003)	100.0(0.0000)	99.98(0.0030)	99.98(0.0002)	99.71(0.0054)	**100.0(0.0000)**
7	99.49(0.0086)	99.99(0.0001)	99.98(0.0002)	99.92(0.0011)	99.98(0.0002)	99.85(0.0017)	100.0(0.0000)	**100.0(0.0000)**
8	98.05(0.0078)	96.09(0.0229)	97.16(0.0110)	95.87(0.0157)	97.00(0.0132)	95.06(0.0536)	97.95(0.0131)	**98.68(0.0089)**
9	99.71(0.0032)	99.84(0.0017)	99.98(0.0002)	99.95(0.0009)	99.89(0.0012)	99.76(0.0022)	99.86(0.0016)	**99.99(0.0001)**
10	96.00(0.0254)	98.69(0.0144)	96.98(0.0216)	98.18(0.0116)	99.50(0.0044)	99.32(0.0048)	99.12(0.0132)	**99.93(0.0006)**
11	97.11(0.0271)	97.65(0.0239)	**98.84(0.0214)**	98.71(0.0117)	97.66(0.0174)	98.08(0.0225)	98.49(0.0206)	96.30(0.0154)
12	98.91(0.0151)	99.08(0.0143)	100.0(0.0000)	99.55(0.0106)	99.77(0.0033)	99.63(0.0055)	99.85(0.0020)	99.97(0.0005)
13	97.24(0.0444)	99.44(0.0085)	98.07(0.0254)	99.58(0.0072)	99.71(0.0049)	**99.84(0.0018)**	99.64(0.0100)	99.53(0.0113)
14	97.03(0.0173)	96.97(0.0166)	98.25(0.0373)	99.12(0.0063)	99.19(0.0099)	98.80(0.0139)	99.22(0.0093)	**99.46(0.0057)**
15	91.08(0.0930)	96.41(0.0226)	**97.31(0.0154)**	96.54(0.0124)	95.54(0.0196)	95.13(0.0374)	96.36(0.0158)	96.54(0.0297)
16	99.94(0.0015)	99.69(0.0072)	98.99(0.0187)	99.22(0.0125)	99.98(0.0003)	99.75(0.0074)	96.42(0.1067)	**99.99(0.0001)**
OA	97.22(0.0180)	98.13(0.0038)	98.68(0.0047)	98.34(0.0033)	98.56(0.0038)	97.91(0.0130)	98.59(0.0109)	**99.09(0.0038)**
AA	97.88(0.0079)	98.52(0.0024)	99.01(0.0045)	98.96(0.0018)	99.08(0.0022)	98.88(0.0038)	98.86(0.0100)	**99.32(0.0021)**
KAPPA	96.94(0.0199)	97.92(0.0042)	98.53(0.0052)	98.14(0.0037)	98.39(0.0042)	97.68(0.0145)	98.43(0.0121)	**98.99(0.0042)**
Params	618.522k	621.407k	205.396k	741.884k	83.771k	67.114k	323.562k	**59.894k**
Runtime	1639.8s	1781.1s	**154.52s**	3230.8s	3016.2s	465.5s	1120.4s	896.0s

TABLE IV
CLASSIFICATION RESULTS ON UP

Methods	DBDA	DBMA	HPDM-SPRN	SSTN	A2S2KResNet	HResNetAM	FECNet	FCAN_AKF
1	95.20(0.0440)	97.90(0.0136)	98.91(0.0051)	99.15(0.0049)	98.25(0.0130)	98.25(0.0067)	98.23(0.0326)	**99.12(0.0044)**
2	98.31(0.0291)	99.35(0.0031)	99.83(0.0020)	99.90(0.0009)	99.74(0.0010)	99.68(0.0018)	99.77(0.0012)	**99.83(0.0034)**
3	85.49(0.0960)	93.85(0.0616)	96.41(0.0186)	94.06(0.0354)	93.71(0.0429)	97.67(0.0226)	97.69(0.0256)	**97.93(0.0139)**
4	94.19(0.0365)	96.99(0.0149)	96.97(0.0186)	96.41(0.0081)	**99.49(0.0029)**	98.26(0.0073)	97.24(0.0217)	98.93(0.0073)
5	99.03(0.0118)	98.63(0.0232)	99.49(0.0016)	99.56(0.0047)	99.24(0.0093)	99.11(0.0150)	98.71(0.0318)	**99.68(0.0012)**
6	98.10(0.0204)	98.98(0.0107)	99.50(0.0029)	99.67(0.0028)	99.23(0.0049)	99.64(0.0034)	**99.71(0.0026)**	99.50(0.0087)
7	98.75(0.0160)	98.56(0.0132)	98.46(0.0015)	99.18(0.0120)	99.42(0.0075)	98.86(0.0183)	95.89(0.1206)	**99.73(0.0078)**
8	88.57(0.0435)	92.46(0.0496)	96.71(0.0225)	97.28(0.0075)	90.78(0.0319)	94.20(0.0383)	93.40(0.0277)	**96.98(0.0099)**
9	95.58(0.0216)	96.92(0.0200)	**98.88(0.0156)**	96.23(0.0580)	98.76(0.0118)	98.72(0.0140)	98.72(0.0089)	97.65(0.0112)
OA	95.85(0.0287)	97.89(0.0072)	98.95(0.0016)	98.88(0.0027)	98.26(0.0025)	98.69(0.0042)	98.38(0.0117)	**99.22(0.0038)**
AA	94.80(0.0216)	97.07(0.0117)	98.40(0.0025)	97.94(0.0080)	97.63(0.0043)	98.27(0.0066)	97.71(0.0166)	**98.82(0.0048)**
KAPPA	94.46(0.0392)	97.20(0.0096)	98.61(0.0021)	98.52(0.0036)	97.70(0.0033)	98.26(0.0055)	97.85(0.0155)	**98.96(0.0050)**
Params	321.491k	324.376k	184.633k	731.986k	221.967k	**34.971k**	171.345k	46.511k
Runtime	555.2s	573.8s	**104.1s**	4431.3	2530.4s	176.9s	486.4s	429.9s

and does not affect the classification performance of the network.

The classification results and parameter quantities of all methods on the SV are shown in Table III. Compared to the IN dataset, the SV dataset has a richer amount of data for training. Therefore, all methods can achieve good classification accuracy on the SV dataset. Nevertheless, compared to other methods, the FCAN_AKF still exhibits more competitive classification results. Similarly, as shown in Table IV, compared to other methods, FCAN_AKF also has significant advantages in classification results on UP. This once again proves that the FCAN_AKF has significant classification performance and good generalization ability.

In addition, the running times of different methods are also shown in Tables II and III. It can be seen that the running time of the proposed FCAN_AKF is only higher than that

of HPDM-SPRN and HResNetAM. For most methods, the running time of FCAN_AKF still has certain advantages.

As shown in Figs. 19–21, in order to compare the classification performance of different methods more intuitively, the classification results of all methods were visualized in this section. The classification map of all methods on the IN is shown in Fig. 19. As shown in Fig. 19, among all the methods, the classification maps of DBMA and DBDA perform poorly compared to other methods. This is because these two methods only simply combine spatial–spectral attention and fail to fully extract HSI features, while the classification maps of other methods all have clear class boundaries. Specifically, compared to classification maps of other methods, the classification map of FCAN_AKF not only has clear class boundaries, but also can better distinguish different classes. This is due to the redundancy information in FCAN_AKF being eliminated by AKF, avoiding mutual interference between different classes. In addition, conclusions similar to those on the IN dataset can also be obtained on the SV and UP datasets.

The number of training samples determines the amount of prior information used for classification in supervised classification tasks. Therefore, the small sample problem has always been one of the main challenges in HSIC. Considering the importance of training samples in supervised classification networks, the classification performance of the proposed method under different training samples was analyzed in this section. Specifically, the proposed FCAN_AKF is compared with seven methods. The classification accuracy of all methods using different proportions of training sample on three datasets is shown in Fig. 22. As shown in Fig. 22(a), on the IN dataset, the classification accuracy of all methods shows an upward trend with the increase of samples. Moreover, compared with other methods, the optimal classification accuracy can be achieved by FCAN_AKF under different proportions of training samples. Specifically, the advantage of FCAN_AKF's classification performance is more significant when the number of training samples is smaller. This indicates that compared to other methods, the FCAN_AKF can also effectively classify under limited training samples. In addition, as the proportions of training samples increase, the classification accuracy of FCAN_AKF is steadily improved, indicating that FCAN_AKF has strong robustness.

IV. CONCLUSION

In order to establish the interdependence between close-range spectral information and long-range spectral information and effectively alleviate the interference of redundant information on the network, an FCAN_AKF is proposed in this article. First, in order to alleviate the problem that it is difficult to establish long-range interaction of spectral information due to the limited receptive field of CNNs, an NBR strategy was designed. After the spectral information is regrouped by NBR, FCAN_AKF can also establish the interdependence between the close-range spectral information and the long-range spectral information in the case of a limited receptive field. In addition, the nonlocal features after spectral regrouping are combined with the local features of the original HSIs by FCAN_AKF to achieve effective classification. Then,

in order to address the interference of redundant information on the network, a DPSSA was proposed and used to capture spectral–spatial attention. DPSSA enhances important feature information and suppresses irrelevant features through autocorrelation. Subsequently, an AKF was designed to further alleviate the interference of redundant information. The redundant information that interferes with network classification can be filtered out by AKF, and important features beneficial to classification can be enhanced. In addition, AKF achieves adaptive filtering of redundant information and gains important features through network training iterations. Finally, the FCAN_AKF proposed in this article has been proven to have better classification performance than some state-of-the-art methods through extensive experiments.

REFERENCES

[1] J. Transon, R. d'Andrimont, A. Maugnard, and P. Defourny, "Survey of current hyperspectral Earth observation applications from space and synergies with Sentinel-2," in *Proc. 9th Int. Workshop Anal. Multitemporal Remote Sens. Images (MultiTemp)*, Brugge, Belgium, Jun. 2017, pp. 1–8.

[2] J. Transon, R. d'Andrimont, A. Maugnard, and P. Defourny, "Survey of hyperspectral Earth observation applications from space in the Sentinel-2 context," *Remote Sens.*, vol. 10, no. 3, p. 157, Jan. 2018.

[3] T. Hou, W. Sun, C. Chen, G. Yang, X. Meng, and J. Peng, "Marine floating raft aquaculture extraction of hyperspectral remote sensing images based decision tree algorithm," *Int. J. Appl. Earth Observ. Geoinf.*, vol. 111, Jul. 2022, Art. no. 102846.

[4] G. Yang, K. Huang, W. Sun, X. Meng, D. Mao, and Y. Ge, "Enhanced mangrove vegetation index based on hyperspectral images for mapping mangrove," *ISPRS J. Photogramm. Remote Sens.*, vol. 189, pp. 236–254, Jul. 2022.

[5] Y. Gu, J. Chanussot, X. Jia, and J. A. Benediktsson, "Multiple kernel learning for hyperspectral image classification: A review," *IEEE Trans. Geosci. Remote Sens.*, vol. 55, no. 11, pp. 6547–6565, Nov. 2017.

[6] M. Gerhards, M. Schlerf, K. Mallick, and T. Udelhoven, "Challenges and future perspectives of multi-/hyperspectral thermal infrared remote sensing for crop water-stress detection: A review," *Remote Sens.*, vol. 11, no. 10, p. 1240, May 2019.

[7] B. Lu, P. Dao, J. Liu, Y. He, and J. Shang, "Recent advances of hyperspectral imaging technology and applications in agriculture," *Remote Sens.*, vol. 12, no. 16, p. 2659, Aug. 2020.

[8] A. S. Sahadevan, "Extraction of spatial–spectral homogeneous patches and fractional abundances for field-scale agriculture monitoring using airborne hyperspectral images," *Comput. Electron. Agricult.*, vol. 188, Sep. 2021, Art. no. 106325.

[9] M. Lv, W. Li, T. Chen, J. Zhou, and R. Tao, "Discriminant tensor-based manifold embedding for medical hyperspectral imagery," *IEEE J. Biomed. Health Informat.*, vol. 25, no. 9, pp. 3517–3528, Sep. 2021.

[10] M. Aref, A.-B. Youssef, and I. El-Sharkawy, "Characterization of normal and malignant breast tissues utilizing hyperspectral images and associated differential spectrum algorithm," *J. Biomed. Photon. Eng.*, vol. 7, no. 2, May 2021, Art. no. 020302.

[11] S. Kumar, J. Ghosh, and M. M. Crawford, "Best-bases feature extraction algorithms for classification of hyperspectral data," *IEEE Trans. Geosci. Remote Sens.*, vol. 39, no. 7, pp. 1368–1379, Jul. 2001.

[12] J. Edirisinghe and S. Khorram, "Hierarchical maximum-likelihood classification for improved accuracies," *IEEE Trans. Geosci. Remote Sens.*, vol. 35, no. 4, pp. 810–816, Jul. 1997.

[13] Y. Chen, N. M. Nasrabadi, and T. D. Tran, "Classification for hyperspectral imagery based on sparse representation," in *Proc. 2nd Workshop Hyperspectral Image Signal Process., Evol. Remote Sens.*, Reykjavik, Iceland: IEEE, Jun. 2010, pp. 1–4.

[14] Y. Duan, H. Huang, and T. Wang, "Semisupervised feature extraction of hyperspectral image using nonlinear geodesic sparse hypergraphs," *IEEE Trans. Geosci. Remote Sens.*, vol. 60, 2022, Art. no. 5515115.

[15] M. E. Paoletti, J. M. Haut, J. Plaza, and A. Plaza, "Deep learning classifiers for hyperspectral imaging: A review," *ISPRS J. Photogramm. Remote Sens.*, vol. 158, pp. 279–317, Dec. 2019.

[16] W. Lv and X. Wang, "Overview of hyperspectral image classification," *J. Sensors*, vol. 2020, Jul. 2020, Art. no. 4817234.

[17] Z. Li, F. Liu, W. Yang, S. Peng, and J. Zhou, "A survey of convolutional neural networks: Analysis, applications, and prospects," *IEEE Trans. Neural Netw. Learn. Syst.*, vol. 33, no. 12, pp. 6999–7019, Dec. 2022.

[18] W. Hu, Y. Huang, L. Wei, F. Zhang, and H. Li, "Deep convolutional neural networks for hyperspectral image classification," *J. Sensors*, vol. 2015, Jul. 2015, Art. no. 258619.

[19] Y. Li, H. Zhang, and Q. Shen, "Spectral–spatial classification of hyperspectral imagery with 3D convolutional neural network," *Remote Sens.*, vol. 9, no. 1, p. 67, Jan. 2017.

[20] Z. Zhong, J. Li, Z. Luo, and M. Chapman, "Spectral–spatial residual network for hyperspectral image classification: A 3-D deep learning framework," *IEEE Trans. Geosci. Remote Sens.*, vol. 56, no. 2, pp. 847–858, Feb. 2018.

[21] W. Wang, S. Dou, Z. Jiang, and L. Sun, "A fast dense spectral–spatial convolution network framework for hyperspectral images classification," *Remote Sens.*, vol. 10, no. 7, p. 1068, Jul. 2018.

[22] J. M. Haut, M. E. Paoletti, J. Plaza, A. Plaza, and J. Li, "Visual attention-driven hyperspectral image classification," *IEEE Trans. Geosci. Remote Sens.*, vol. 57, no. 10, pp. 8065–8080, Oct. 2019.

[23] X. Mei et al., "Spectral–spatial attention networks for hyperspectral image classification," *Remote Sens.*, vol. 11, no. 8, p. 963, Apr. 2019.

[24] H. Sun, X. Zheng, X. Lu, and S. Wu, "Spectral–spatial attention network for hyperspectral image classification," *IEEE Trans. Geosci. Remote Sens.*, vol. 58, no. 5, pp. 3232–3245, May 2020.

[25] C. Pu, H. Huang, and L. Yang, "An attention-driven convolutional neural network-based multi-level spectral–spatial feature learning for hyperspectral image classification," *Expert Syst. Appl.*, vol. 185, Dec. 2021, Art. no. 115663.

[26] W. Ma, Q. Yang, Y. Wu, W. Zhao, and X. Zhang, "Double-branch multi-attention mechanism network for hyperspectral image classification," *Remote Sens.*, vol. 11, no. 11, p. 1307, Jun. 2019.

[27] R. Li, S. Zheng, C. Duan, Y. Yang, and X. Wang, "Classification of hyperspectral image based on double-branch dual-attention mechanism network," *Remote Sens.*, vol. 12, no. 3, p. 582, Feb. 2020.

[28] Z. Zhong, Y. Li, L. Ma, J. Li, and W.-S. Zheng, "Spectral–spatial transformer network for hyperspectral image classification: A factorized architecture search framework," *IEEE Trans. Geosci. Remote Sens.*, vol. 60, 2022, Art. no. 5514715.

[29] Z. Xue, X. Yu, B. Liu, X. Tan, and X. Wei, "HResNetAM: Hierarchical residual network with attention mechanism for hyperspectral image classification," *IEEE J. Sel. Topics Appl. Earth Observ. Remote Sens.*, vol. 14, pp. 3566–3580, 2021.

[30] X. Zheng, H. Sun, X. Lu, and W. Xie, "Rotation-invariant attention network for hyperspectral image classification," *IEEE Trans. Image Process.*, vol. 31, pp. 4251–4265, 2022.

[31] S. Mei, X. Li, X. Liu, H. Cai, and Q. Du, "Hyperspectral image classification using attention-based bidirectional long short-term memory network," *IEEE Trans. Geosci. Remote Sens.*, vol. 60, 2022, Art. no. 5509612.

[32] J. He, L. Zhao, H. Yang, M. Zhang, and W. Li, "HSI-BERT: Hyperspectral image classification using the bidirectional encoder representation from transformers," *IEEE Trans. Geosci. Remote Sens.*, vol. 58, no. 1, pp. 165–178, Jan. 2020.

[33] X. Hu, W. Yang, H. Wen, Y. Liu, and Y. Peng, "A lightweight 1-D convolution augmented transformer with metric learning for hyperspectral image classification," *Sensors*, vol. 21, no. 5, p. 1751, Mar. 2021.

[34] Y. Qing, W. Liu, L. Feng, and W. Gao, "Improved transformer net for hyperspectral image classification," *Remote Sens.*, vol. 13, no. 11, p. 2216, Jun. 2021.

[35] X. Hu, T. Li, T. Zhou, Y. Liu, and Y. Peng, "Contrastive learning based on transformer for hyperspectral image classification," *Appl. Sci.*, vol. 11, no. 18, p. 8670, Sep. 2021.

[36] X. He, Y. Chen, and Z. Lin, "Spatial–spectral transformer for hyperspectral image classification," *Remote Sens.*, vol. 13, no. 3, p. 498, Jan. 2021.

[37] D. Hong et al., "SpectralFormer: Rethinking hyperspectral image classification with transformers," *IEEE Trans. Geosci. Remote Sens.*, vol. 60, 2022, Art. no. 5518615.

[38] X. Xue, H. Zhang, B. Fang, Z. Bai, and Y. Li, "Grafting transformer on automatically designed convolutional neural network for hyperspectral image classification," *IEEE Trans. Geosci. Remote Sens.*, vol. 60, 2022, Art. no. 5531116.

[39] C. Shi, H. Wu, and L. Wang, "A positive feedback spatial–spectral correlation network based on spectral slice for hyperspectral image classification," *IEEE Trans. Geosci. Remote Sens.*, vol. 61, 2023, Art. no. 5503417.

[40] X. Jia and J. A. Richards, "Segmented principal components transformation for efficient hyperspectral remote-sensing image display and classification," *IEEE Trans. Geosci. Remote Sens.*, vol. 37, no. 1, pp. 538–542, Jan. 1999.

[41] J. Zabalza et al., "Novel segmented stacked autoencoder for effective dimensionality reduction and feature extraction in hyperspectral imaging," *Neurocomputing*, vol. 185, pp. 1–10, Apr. 2016.

[42] G. Sun et al., "Deep fusion of localized spectral features and multi-scale spatial features for effective classification of hyperspectral images," *Int. J. Appl. Earth Observ. Geoinf.*, vol. 91, Sep. 2020, Art. no. 102157.

[43] H. Wu, C. Shi, L. Wang, and Z. Jin, "A cross-channel dense connection and multi-scale dual aggregated attention network for hyperspectral image classification," *Remote Sens.*, vol. 15, no. 9, p. 2367, Apr. 2023.

[44] R. Liu, W. Cai, G. Li, X. Ning, and Y. Jiang, "Hybrid dilated convolution guided feature filtering and enhancement strategy for hyperspectral image classification," *IEEE Geosci. Remote Sens. Lett.*, vol. 19, 2022, Art. no. 5508105.

[45] X. Zhang, S. Shang, X. Tang, J. Feng, and L. Jiao, "Spectral partitioning residual network with spatial attention mechanism for hyperspectral image classification," *IEEE Trans. Geosci. Remote Sens.*, vol. 60, 2022, Art. no. 5507714.

[46] S. K. Roy, S. Manna, T. Song, and L. Bruzzone, "Attention-based adaptive spectral–spatial kernel ResNet for hyperspectral image classification," *IEEE Trans. Geosci. Remote Sens.*, vol. 59, no. 9, pp. 7831–7843, Sep. 2021.

[47] C. Shi, D. Liao, T. Zhang, and L. Wang, "Hyperspectral image classification based on expansion convolution network," *IEEE Trans. Geosci. Remote Sens.*, vol. 60, 2022, Art. no. 5528316.

Cuiping Shi (Member, IEEE) received the M.S. degree from Yangzhou University, Yangzhou, China, in 2007, and the Ph.D. degree from the Harbin Institute of Technology (HIT), Harbin, China, in 2016.

From 2017 to 2020, she held a post-doctoral research at the College of Information and Communications Engineering, Harbin Engineering University, Harbin. She is currently a Professor with the Department of Communication Engineering, Qiqihar University, Qiqihar, China. Since 2023, she has been working with the College of Information Engineering, Huzhou University, Huzhou, China. She has authored two academic books about remote sensing image processing and more than 80 articles in journals and conference proceedings. Her main research interests include remote sensing image processing, pattern recognition, and machine learning.

Dr. Shi won the Nomination Award of Excellent Doctoral Dissertation of Harbin University of Technology (HIT) in 2016, for her doctoral dissertation.

Haiyang Wu received the bachelor's degree from Jinjiang College, Sichuan University, Meishan, Sichuan, China, in 2021. He is currently pursuing the master's degree with Qiqihar University, Qiqihar, China.

His research interests include hyperspectral image processing and machine learning.

Liguo Wang (Member, IEEE) received the M.S. and Ph.D. degrees in signal and information processing from the Harbin Institute of Technology, Harbin, China, in 2002 and 2005, respectively.

From 2006 to 2008, he held a post-doctoral research position at the College of Information and Communications Engineering, Harbin Engineering University, Harbin, where he is currently a Professor. Since 2020, he has been working with the College of Information and Communication Engineering, Dalian Nationalities University, Dalian, China. He has authored two books about hyperspectral image processing and more than 130 articles in journals and conference proceedings. His main research interests include remote sensing image processing and machine learning.

检 索 报 告

一、检索要求

1. 委 托 人：石翠萍 Shi, CP (Shi, Cuiping)

2. 委托单位：齐齐哈尔大学

3. 检索目的：论文被 SCI-E 收录情况

二、检索范围

Science Citation Index Expanded (SCI-EXPANDED)	1990-present	网络版
JCR-(Journal Citation Reports)	2022	网络版
中国科学院文献情报中心期刊分区表(升级版)	2022	网络版

三、检索结果

委托人提供的**1**篇论文被SCI-E收录，论文被收录、所在期刊的JCR影响因子、中科院期刊分区(升级版)情况见附件一。

特此证明！

检索报告人：杨茗惠

东北师范大学科技查新咨询中心

教育部科技查新工作站(L24)

2023 年 11 月 20 日

附件一：SCI-E收录情况

作者: **Shi, CP (Shi, Cuiping)**; Wu, HY (Wu, Haiyang); Wang, LG (Wang, Liguo)

Web of Science 核心合集中的 "被引频次": 0

被引频次合计: 0

使用次数 (最近 180 天): 0

使用次数 (2013 年至今): 0

引用的参考文献数: 47

摘要: In recent years, convolutional neural networks (CNNs) have been widely used in hyperspectral image classification (HSIC). However, the size of the convolutional kernel in CNNs is fixed, which makes it difficult to capture the dependence of long-range feature information. In addition, the extracted features often contain a large amount of redundant information. In order to alleviate these issues, a feature complementary attention network based on adaptive knowledge filtering (FCAN_AKF) is proposed in this article. First, in order to alleviate the problem that CNNs are difficult to capture the dependence between close-range and long-range spectral features due to the limited receptive field, a nonlocal band regrouping (NBR) strategy is designed. NBR enables CNN to capture nonlocal spectral features in a limited receptive field to establish the interdependence between close-range and long-range spectral features. In addition, the nonlocal features extracted after using NBR and the local features of the original hyperspectral image are integrated to achieve complementation between nonlocal features and local features. Then, in order to eliminate the interference of redundant information on the network, a dual-pyramid spectral-spatial attention (DPSSA) module is proposed and used to capture spectral-spatial attention. Next, an adaptive knowledge filter (AKF) is designed, which can adaptively further filter out redundant information and enhance feature information that is beneficial for classification. Finally, extensive experiments were conducted on three challenging datasets, demonstrating that the proposed method has stronger competitiveness compared to some state-of-the-art HSIC methods.

入藏号: WOS:001087763100015

语言: English

文献类型: Article

作者关键词: Feature extraction; Three-dimensional displays; Data mining; Convolution; Interference; Hyperspectral imaging; Convolutional neural networks; Adaptive knowledge filter (AKF); convolutional neural network (CNN); dual-pyramid spectral-spatial attention (DPSSA); hyperspectral image classification (HSIC); nonlocal band regrouping (NBR)

KeyWords Plus: RESIDUAL NETWORK

地址: [Shi, Cuiping] Huzhou Univ, Qiuzhen Coll, Huzhou 313000, Peoples R China.

[Shi, Cuiping; Wu, Haiyang] Qiqihar Univ, Dept Commun Engn, Qiqihar 161000, Peoples R China.

[Wang, Liguo] Dalian Nationalities Univ, Coll Informat & Commun Engn, Dalian 116000, Peoples R China.

通讯作者地址: Shi, CP (通讯作者), Huzhou Univ, Qiuzhen Coll, Huzhou 313000, Peoples R China.

电子邮件地址: shicuiping@qqhru.edu.cn; 2021910323@qqhru.edu.cn; wangliguo@hrbeu.edu.cn

Affiliations: Huzhou University; Qiqihar University; Dalian Minzu University

Web of Science Index: Science Citation Index Expanded (SCI-EXPANDED)

Web of Science 类别: Geochemistry & Geophysics; Engineering, Electrical & Electronic; Remote Sensing; Imaging Science & Photographic Technology

研究方向: Geochemistry & Geophysics; Engineering; Remote Sensing; Imaging Science & Photographic Technology

IDS 号: U9EP1

基金资助致谢:

输出日期: 2023-11-20

期刊影响因子 ™ 2022：8.2

中国科学院文献情报中心期刊分区(升级版, 2022)截图如下：

IEEE TRANSACTIONS ON GEOSCIENCE AND REMOTE SENSING

刊名	IEEE TRANSACTIONS ON GEOSCIENCE AND REMOTE SENSING
年份	2022
ISSN	0196-2892
Review	否
Open Access	否
Web of Science	SCIE

	学科	分区	Top期刊
大类	工程技术	1	是
小类	GEOCHEMISTRY & GEOPHYSICS 地球化学与地球物理	1	
	ENGINEERING, ELECTRICAL & ELECTRONIC 工程：电子与电气	2	
	IMAGING SCIENCE & PHOTOGRAPHIC TECHNOLOGY 成像科学与照相技术	2	
	REMOTE SENSING 遥感	2	

The End